11-2009

# The upper lithostratigraphic unit of ANDRILL AND-2A core (Southern McMurdo Sound, Antarctica): Local Pleistocene volcanic sources, paleoenvironmental implications and subsidence in the southern Victoria Land Basin

Paola Del Carlo
*Istituto Nazionale di Geofisica e Vulcanologia, Pisa, Italy*, delcarlo@pi.ingv.it

Kurt Panter
*Bowling Green State University*, kpanter@bgsu.edu

Kari Bassett
*University of Canterbury, New Zealand*, kari.bassett@canterbury.ac.nz

Laura Bracciali
*Università di Pisa*, bracciali@dst.unipi.it

Gianfranco Di Vincenzo
*Istituto di Geoscienze e Georisorse, CNR, Pisa, Italy*, g.divincenzo@igg.cnr.it

*See next page for additional authors*

Published in *Global and Planetary Change* 69:3 (November 2009), pp. 142–161; doi:10.1016/j.gloplacha.2009.09.002

Submitted March 16, 2009; accepted September 18, 2009; published online 1 October 1, 2009.

Presented at Cenozoic Antarctic glacial history, EGU meeting (http://0-meetings.copernicus.org/egu2008/ )
and International Geological Congress (IGC) Conference (http://www.33igc.org/ )

# The upper lithostratigraphic unit of ANDRILL AND-2A core (Southern McMurdo Sound, Antarctica): Local Pleistocene volcanic sources, paleoenvironmental implications and subsidence in the southern Victoria Land Basin

P. Del Carlo,[1] K. S. Panter,[2] K. Bassett,[3] L. Bracciali,[4] G. Di Vincenzo,[5] and S. Rocchi [4]

1. Istituto Nazionale di Geofisica e Vulcanologia, Sezione di Pisa, via della Faggiola 32, I-56126 Pisa, Italy
2. Department of Geology, Bowling Green State University, Bowling Green, OH, 43403, USA
3. Department of Geological Science, University of Canterbury, Private Bag 4800, Christchurch, New Zealand
4. Dipartimento di Scienze della Terra, Università di Pisa, Via S. Maria 53, I-56126 Pisa, Italy
5. Istituto di Geoscienze e Georisorse, CNR, via Moruzzi 1, I-56100 Pisa, Italy

*Corresponding author* — P. Del Carlo, tel 39 050 8311943, fax 39 050 8311942, email delcarlo@pi.ingv.it

**Abstract**

We report results from the study of the uppermost 37 m of the Southern McMurdo Sound (SMS) AND-2A drill core, corresponding to the lithostratigraphic unit 1 (LSU 1), the most volcanogenic unit within the core. We present data on the age, composition, volcanological and depositional features of the volcanic sedimentary and tephra deposits of LSU 1 and discuss their source, mechanisms of emplacement and environment of deposition.

Sedimentary features and compositional data indicate shallow water sedimentation for the whole of LSU 1. Most of LSU 1 deposits are a mixture of near primary volcanic material with minor exotic clasts derived from the Paleozoic crystalline basement rocks. Among volcanic materials, glassy particles are the most abundant. They were produced by mildly explosive basaltic eruptions occurring in subaerial and subaqueous environments. The Dailey Islands group, 13 km south-southwest of the SMS drill-site, has been identified as a possible source for the volcanics on the basis of similarity in composition and age. $^{40}Ar$–$^{39}Ar$ laser step-heating analyses on a lava sample from Juergens Island yields an age of 775 ± 22 ka. Yet because of the minimal reworking features of vitriclasts, preservation of fragile structures in volcaniclastic sediments and evidence for volcanic seamounts to the north of the Dailey Islands, it is likely that some of the material originated also from vents close to the drill-site.

Evidence for local volcanic sources and for deposition of sediments in a shallow marine environment provides indications about the local paleogeography and implications for the subsidence history of the southern Victoria Land Basin from Pleistocene to Recent.

**Keywords:** Antarctica, volcaniclastic sediments, Erebus Volcanic Province, paleoenvironment reconstruction, Victoria Land Basin

## 1. Introduction

The Antarctic continent is a highly sensitive and suitable area to investigate and compare the present environmental conditions with records of past changes. Particularly, records of modifications in the extent and thickness of terrestrial and marine ice cover can be exploited as environmental and climate proxies. Key areas in Antarctica are the marine depositional environments close to the continent, where sediment input is directly related to environmental changes in the terrestrial environment. Most of these areas have been affected episodically during the Cenozoic by tectonic and volcanic activity linked to the West Antarctic Rift System. It is therefore crucial to develop a reconstruction of the influence of volcanic activity on the paleoenvironment, landscape, and basin development.

The ANDRILL Program represents a multinational effort to investigate these themes. The aim of this research program is to recover and examine extended drill cores from the Antarctic coastal sedimentary basins, building up stratigraphic records that document key events in Antarctica's Cenozoic climatic and glacial history, as well as the volcanic and tectonic development of this portion of the West Antarctic Rift System and Transantarctic Mountains (Harwood et al., 2008).

During the fourth International Polar Year (2007), ANDRILL's Southern McMurdo Sound (SMS) Project successfully cored the AND-2A hole in the Ross Sea approximately 50 km NW of Hut Point Peninsula on Ross Island (77°45.488'S, 165°16.605'E, Figure 1). The drilling operated on the surface of an 8.4 meter thick multi-year sea-ice platform floating over 384 m of water. The drilling program recovered an excellent quality core (98% recovery) comprising marine and glacimarine sediments down to a depth of 1138.54 m below sea floor (mbsf). This is the second deepest drill hole on the Antarctic continent and is exceeded only by ANDRILL's first drill hole (AND-1B, McMurdo Ice

Shelf Project), which reached a total depth of 1284.87 m in December, 2006 (Florindo et al., 2008). Thus, the sedimentary archive provided by the ANDRILL AND-2A core represents a valuable record from which past climatic, tectonic and volcanological changes in the southern high latitudes can be reconstructed.

In this paper we report a detailed study of the uppermost lithostratigraphic unit (LSU 1) of the AND-2A core, corresponding to the top 37 m. This unit consists mostly of volcaniclastic deposits and nearly primary tephra; it is the most volcanogenic among the 14 lithostratigraphic units defined (Fielding et al., 2008b; Panter et al., 2008). We present data on composition and volcanological and depositional features of the sedimentary materials in order to draw conclusions regarding their source, mechanisms of emplacement and environment of deposition. In addition, with the aim of comparing volcanogenic clasts of LSU 1 with known volcanic deposits near the AND-2A site, we also report petrographic, geochemical and $^{40}Ar$–$^{39}Ar$ data on one sample from the Dailey Islands group, located a few kilometers south–southwest of the SMS drill-site. The results are used to infer local paleogeography and tectonic development of the southern Victoria Land Basin.

## 2. Geological setting

The McMurdo Sound region has a rich history of rift-related alkaline volcanism. Large volcanoes or volcanic complexes include Mounts Erebus, Terror and Bird, which form Ross Island, and Mount Discovery, Minna Bluff and Mount Morning located on the mainland (Figure 1). These volcanoes, and many smaller volcanic centers (e.g., Brown Peninsula, White and Black Islands) and volcanic fields (e.g., the foothills of Royal Society Range, Wright-Taylor Valleys, Dailey Islands), are part of the Erebus Volcanic Province (Kyle and Cole, 1974; Kyle, 1990). This province represents one of the largest areas of exposed Late Cenozoic volcanic rocks in Antarctica, with an extended Miocene to present re-

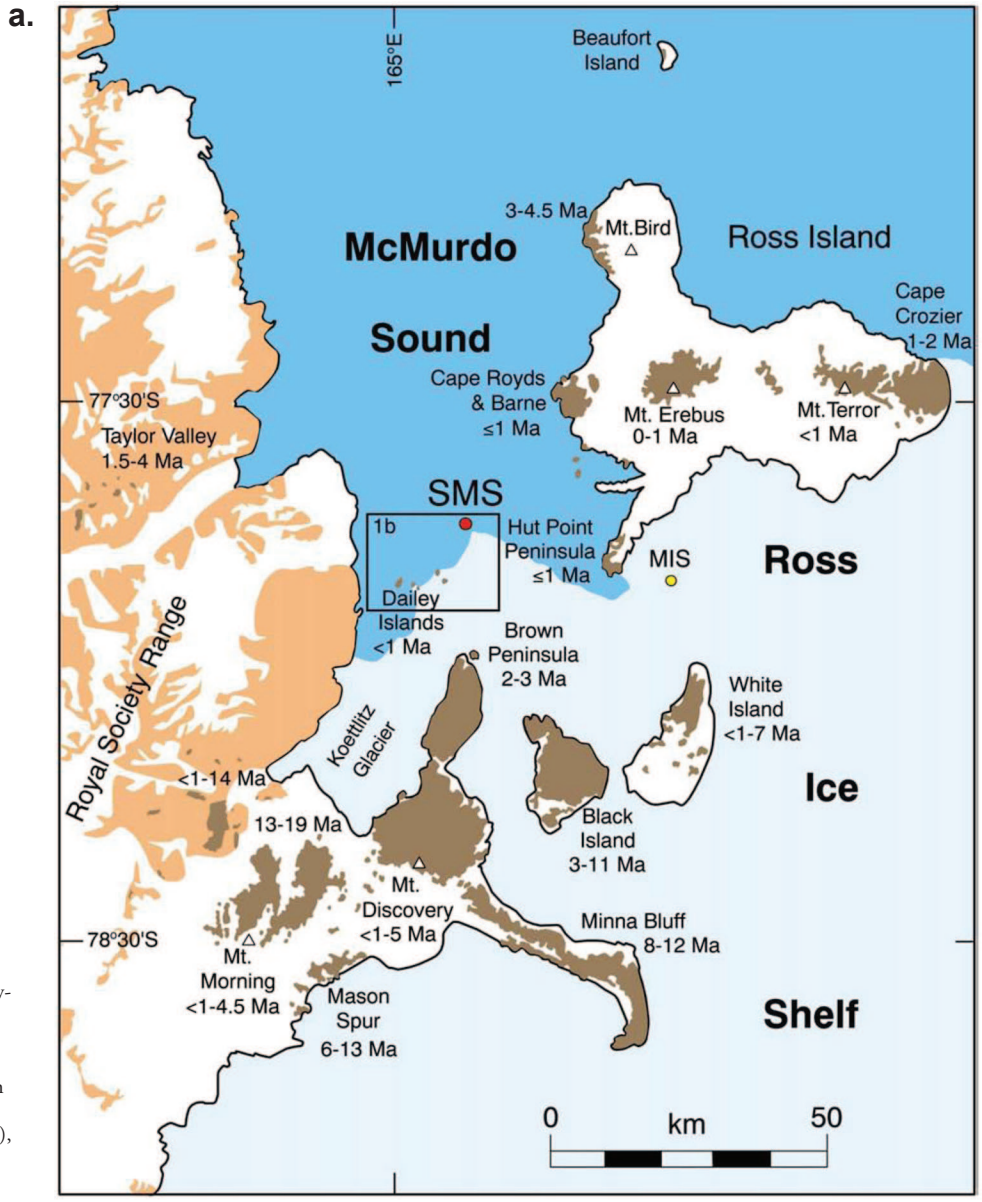


**Figure 1.** a) Map of McMurdo Sound area showing the ANDRILL SMS and MIS drill-sites relative to exposed deposits of the Erebus Volcanic Province. Ages are from Kyle (1990 and references therein), with additional dates from Wilch et al. (1993), Esser et al. (2004), Harpel et al. (2004), Tauxe et al. (2004), Cooper et al. (2007), Fargo et al. (2008), and Lawrence et al. (2009), and this study; *(continued)*

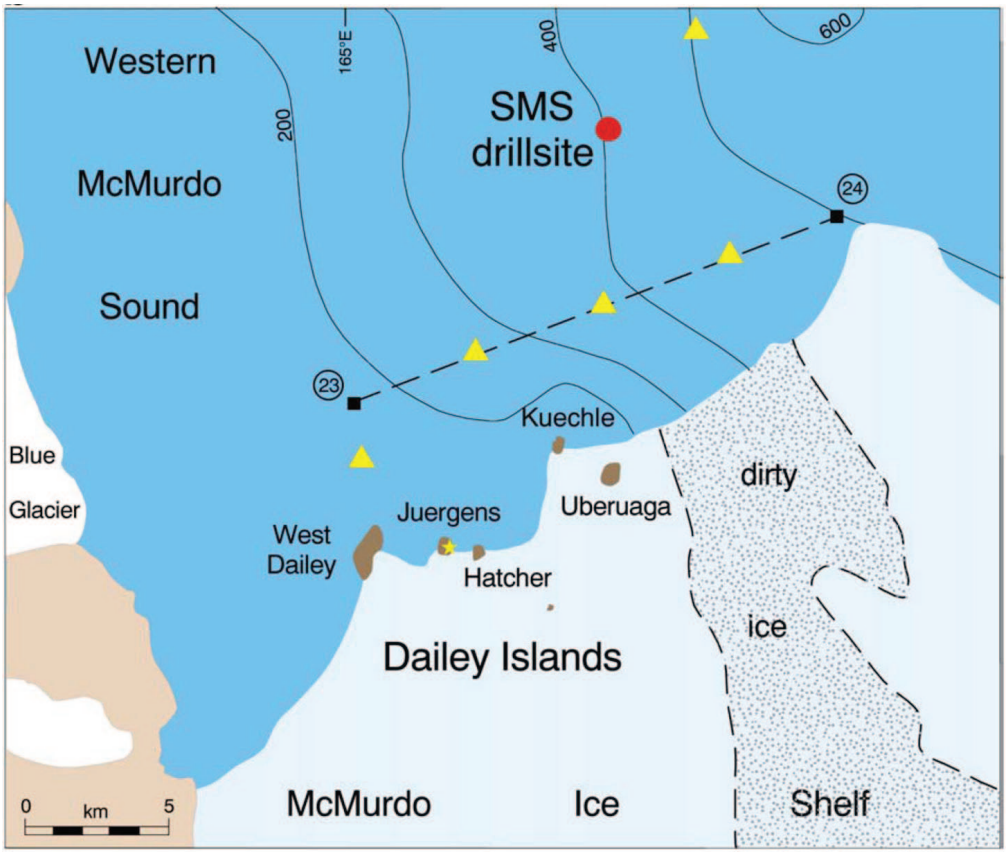


**Figure 1.** (continued) b) Detail of a) showing the SMS drill-site relative to Dailey Islands. Seafloor bathymetry and locations of grab/core stations 23 and 24 are taken from Barrett et al. (1983). Triangles mark the locations of shallow soundings that Barrett et al. (1983) interpreted as five submarine volcanic cones. The top of each peak lies at water depths between 100 and 200 mbsl. The star on Juergens Island marks the location of the sample collected for petrography, geochemistry and dating.

cord of eruptive activity. Volcanic deposits on land range in age from ~ 19 Ma to current Strombolian-style activity issuing from a convecting phonolitic lava lake located in the summit crater of the Erebus volcano (Oppenheimer and Kyle, 2008). Evidence for older volcanic activity in the area comes from drill cores (CIROS-1, MSSTS-1, Cape Roberts and AND-2A drillcores), which extend the volcanic history to 26–20 Ma (Gamble et al., 1986; Barrett, 1987; McIntosh, 1998; McIntosh, 2000; Acton et al., 2008; Di Vincenzo et al., 2009). The whole set of $^{40}Ar$–$^{39}Ar$ data so far available on volcanogenic samples from the AND-2A core, including those from the LSU 1, are reported in a separate paper (Di Vincenzo et al., submitted).

Compositionally, most of deposits in the Erebus Volcanic Province belong to the strongly silica-undersaturated basanite to phonolite alkaline series. There are also present in much lesser volume the moderately silica-undersaturated alkali basalt to trachyte alkaline series, along with rare silica-oversaturated and peralkaline trachytes. This distinction appears to be temporally and spatially controlled, with the majority of moderately undersaturated and oversaturated compositions restricted to deposits that are 11 Ma or older, and located in the southwest corner of the province at Mason Spur and near the base of Mt. Morning (Kyle, 1990). Apart from the tephriphonolite and phonolite compositions erupted on the flanks and summit of Mt. Erebus, most of the young volcanism (≤ 1 Ma) occurred in small-volume basaltic eruptions from clusters of cinder cones and associated lavas in many areas. One of these cinder cone fields is the Dailey Island group, which is located just south of the SMS drill-site (Figure 1).

The Dailey Islands group is the most proximal volcanism to the SMS site and is located in McMurdo Sound approximately 35 km west-southwest of Hut Point and 13 km to the south–southwest of the SMS drillsite (Figure 1a). The group consists of five small volcanic islands (West Dailey, Juergens, Hatcher, Uberuaga and Kuechle) that protrude through the edge of the Ross Ice Shelf (Figure 1b). The islands represent heavily eroded remnants of basaltic cinder cone and lava deposits and have been overridden by past glaciations (Mankinen and Cox, 1988; Denton and Marchant, 2000). Paleomagnetic studies of volcanic rocks from two of the Dailey Islands (Juergens and Kuechle) reveal normal polarities (Mankinen and Cox, 1988; Tauxe et al., 2004). Tauxe et al. (2004) also obtained a $^{40}Ar$–$^{39}Ar$ age of 0.78 ± 0.04 Ma (recalculated using an age of 28.34 Ma for the fluence monitor TCs, according to Renne et al., 1998) on a dyke sample from Juergens Island, which is consistent with eruption during the oldest portion of the Brunhes Chron. This places the age of the Dailey Islands within the timeframe relevant to the uppermost stratigraphic unit (LSU 1) of the SMS core treated herein.

All of the volcanic deposits in the Erebus Volcanic Province are located in and around the southern portion of the Victoria Land Basin, one of four major rift-related basins within the Ross Sea. Extension and rifting began during the Late Mesozoic and further developed through the Cenozoic to the early Neogene, when a change to transtension and strike-slip faulting in the southern portion of the Victoria Land Basin formed the Terror Rift (Wilson, 1995, 1999). Evidence for neotectonic normal-fault to strike-slip fault regime within the Terror Rift is presented by Paulsen and Wilson (2009). The cause of the volcanism here and for the rest of the West Antarctic rift is still under discussion (Finn et al., 2005). Plume-driven rifting and volcanism has been proposed (Behrendt et al., 1991; Kyle et al., 1992), and more recently, alternative explanations promote decompression melting of enriched metasomatized continental lithosphere by intraplate stresses (Rocchi et al., 2002, 2003, 2005), and/or by contact with warm Pacific mantle (Finn et al., 2005). In this context, the ANDRILL project also contributes to the knowledge of possible feedback mechanisms between volcanism, tectonism and climate.

## 3. Materials and methods

On the basis of significant lithological changes observed downcore, the sediments of AND-2A core were subdivided into 14 lithostrati-

graphic units (LSUs) with emphasis on diamictite and associated lithologies, relative to other terrigenous clastic and volcanogenic lithologies (Fielding et al., 2008b). LSU 1 is the uppermost unit from 0.0 to 37.07 mbsf (depths are recorded as meters below sea floor and relate to the depths recorded while drilling) and comprises a succession of mixed volcanic rocks ranging from near primary tephra to reworked volcanic sand to diamicton and breccia (Figure 2). The poor recovery (~ 60%) of this unit relative to the rest of the core is due to the weak induration of some coarse deposits and its position at the top of the core. Some intervals were recovered in composite bags (bagged samples), in which

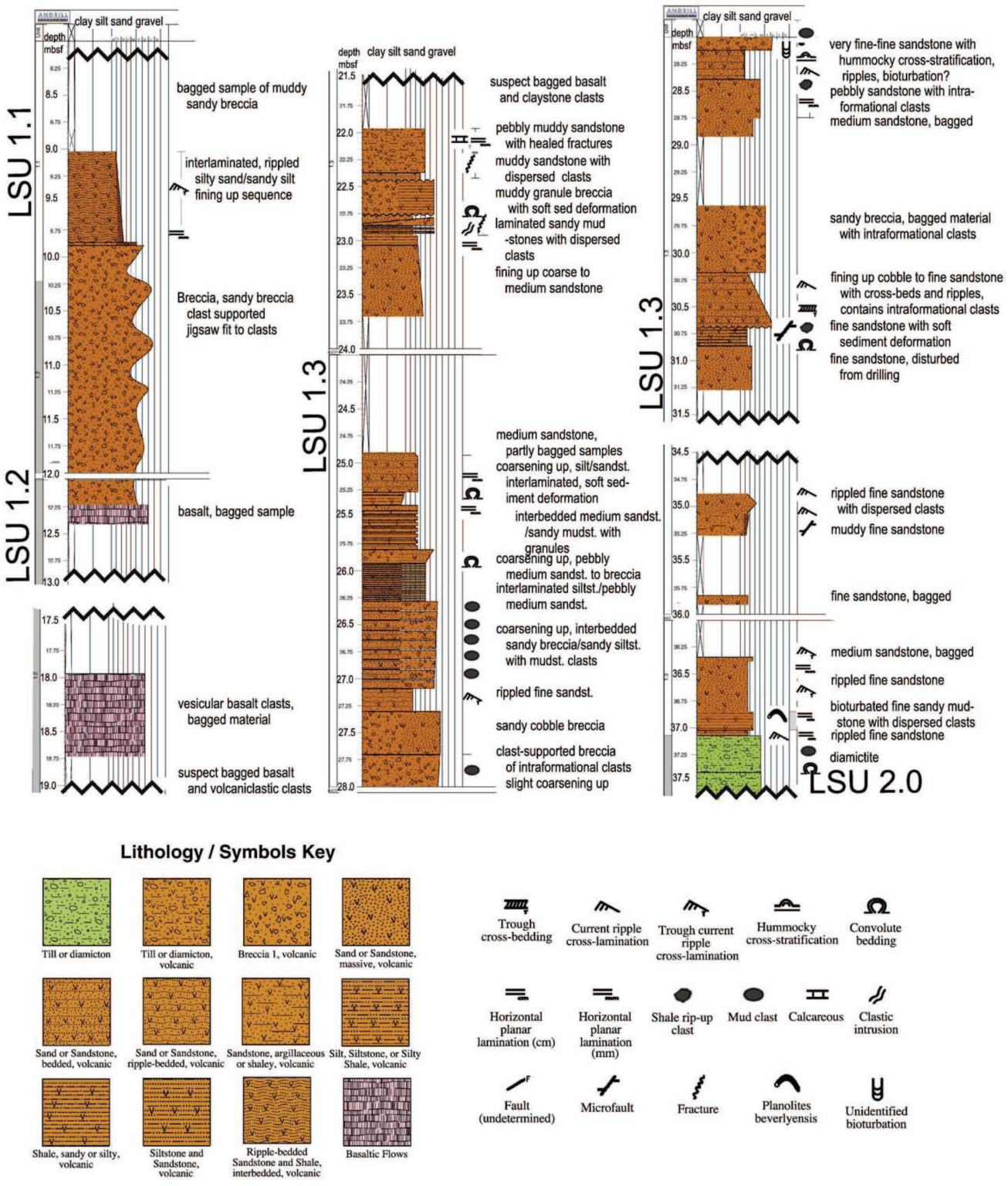


**Figure 2.** Lithostratigraphic section of LSU 1.

**Table 1.** Description of LSU1 samples studied in this work.

| LSU 1 | Top | Bottom | Lithology |
|---|---|---|---|
| 1.1 | 8.88 | 9.02 | Phonolitye, trachyte, tholeiitic basalt and hyaloclastite clasts |
| 1.1 | 9.34 | 9.36 | Olive-yellow laminated volcanic sand |
| 1.1 | 9.40 | 9.43 | in part trough cross-laminated |
| 1.1 | 9.61 | 9.63 | |
| 1.1 | 10.07 | 10.09 | Brown coarse volcanic gravel and sand |
| 1.2 | 10.22 | 10.44 | Basaltic lava clast |
| 1.2 | 10.79 | 10.81 | Basaltic lava clast in volcanic breccia |
| 1.2 | 11.36 | 11.38 | Black volcanic breccia |
| 1.2 | 11.94 | 11.96 | Basaltic lava clast in breccia showing reddish rind |
| 1.2 | 12.23 | 12.41 | Hawaiitic lava clast |
| 1.2 | 18.03 | 18.25 | Basanitic lava clast |
| 1.2 | 18.63 | 18.73 | Tephritic lava clast |
| 1.2 | 18.69 | 18.73 | Basanitic lava clast |
| 1.3 | 22.11 | 22.14 | Sandy siltstone with sideromelane, tachylite and minor lava clasts |
| 1.3 | 22.60 | 22.64 | Black fine-grained volcanic breccia |
| 1.3 | 22.80 | 22.84 | Hyaloclastite in contact with a volcaniclastic sandstone |
| 1.3 | 23.20 | 23.23 | Reddish medium sand including portions of a cemented sandstone |
| 1.3 | 23.62 | 23.65 | Black medium- to coarse-grained sand |
| 1.3 | 24.98 | 25.01 | Grayish fine- to medium-grained sand |
| 1.3 | 25.54 | 25.57 | Reddish fine-grained laminated sand |
| 1.3 | 25.81 | 25.84 | Reddish medium-grained sand and subrounded glassy granules |
| 1.3 | 25.95 | 25.98 | Grayish laminated medium-grained sand |
| 1.3 | 26.33 | 26.36 | Olive-gray volcanic sandy breccia |
| 1.3 | 27.19 | 27.23 | Greenish fine-grained laminated volcanic sandstone |
| 1.3 | 27.39 | 27.45 | Basanite lava clast in volcanic sandy breccia |
| 1.3 | 27.65 | 27.68 | Tan sandstone with black scoria lapilli |
| 1.3 | 28.21 | 28.24 | Black-greenish laminated fine hyaloclastite sandstone |
| 1.3 | 28.55 | 28.59 | Reddish medium-grained volcanic sand |
| 1.3 | 29.95 | 29.98 | Volcanic sandy breccia |
| 1.3 | 30.42 | 30.45 | Dark gray medium-grained volcanic sand |
| 1.3 | 30.91 | 30.95 | Black medium-grained volcanic sand |
| 1.3 | 35.02 | 35.05 | Rippled volcanic sandstone |
| 1.3 | 36.32 | 36.35 | Crossed-laminated volcanic siltstone |
| 1.3 | 36.62 | 36.65 | Black medium-grained volcanic sand |
| 1.3 | 37.07 | 37.10 | Greenish-brown laminated sand |

case the stratigraphic relationships are not recognizable. Diagenesis occurred in fine-grained layers or breccia deposits with fine-grained matrices. Nevertheless, deposits in LSU 1 show a wide range of features, providing significant information about volcanism and paleoenvironment during the middle to late Neogene period in the McMurdo Sound area.

Deposits have been described and sampled (Table 1) in order to determine their sedimentologic and volcanological characteristics and petrochemical composition by means of analytical and componentry analyses. Sand samples were cleaned in an ultrasonic bath to remove impurities and dried at 60 °C. Preliminary observations under stereomicroscope were done to qualitatively evaluate the different components and select samples for microprobe analysis. Polished thin sections were prepared for petrographic, microanalytical and component study.

Component abundance and morphology of particles, and variations in their relative proportion, all furnish useful information on their origin and sedimentation processes. Modal analysis was carried out on 9 sands and 2 sandstones from LSU 1 according to the Gazzi-Dickinson technique (Gazzi, 1966; Dickinson, 1970; Table 2 and Figure 3 & Figure 4), with the aim of quantitatively characterizing the compositional variability of the detritus recovered from LSU 1. Sands were impregnated with Epofix resin and prepared as standard thin sections. In order to allow the comparison between loose (a few partly lithified) sands and sandstones, in each thin section 500 grains were counted using optical microscopy, and the point counts were recalculated to percentages.

Morphological analyses of grains were performed using stereomicroscope and SEM-EDS at the Dipartimento di Scienze della Terra, Università di Pisa. Mineral analyses were carried out on carbon coated thin sections, using a Philips XL30 SEM equipped with an EDAX DX4i microanalytical system (20 kV accelerating potential, 10 nA beam current, 0.5 μm beam diameter).

Whole-rock major element composition was determined for fused 12 lava samples (Table 3) using a X-Ray Fluorescence (XRF, ARL 9400 XP spectrometer) at the Dipartimento di Scienze della Terra, Università di Pisa, following the procedure of Tamponi et al. (2003). Loss on Ignition (LOI) was determined gravimetrically on preheated powders (110 °C) after 1 h ignition at 1000 °C in a microwave furnace.

Glassy fragments (Table 4), minerals and alteration phases were analyzed for major elements on polished thin sections at the HPHT Laboratory of Istituto Nazionale di Geofisica e Vulcanologia (Sezione di Roma) using a JEOL JXA 8200 equipped with 5 wavelength-dispersive spectrometers (WDS) and an energy-dispersive analyzer (accelerating voltage 15 kV, beam current 12 nA, probe diameter 5 μm, acquisition time 10 s and 5 s for peak and background respectively).

Sample preparation and $^{40}Ar$–$^{39}Ar$ laser step-heating analyses were carried out at the IGG-CNR laboratory and followed the procedures described in Di Vincenzo and Skála (2009) and Di Vincenzo et al. (submitted). A comparison sample from the Dailey Islands was irradiated for 2 h in the core of the TRIGA reactor at the Università di Pavia (Italy) along with the fluence monitor Fish Canyon sanidine (FCs). Data corrected for post-irradiation decay, mass discrimination effects, isotopes derived from interference reactions and blanks are listed in Table 5. Ages are relative to an age of 28.03 Ma for FCs (Jourdan and Renne, 2007), and errors are given at 2σ. Errors on step ages are analytical errors, including in-run statistics and uncertainties in the discrimination factor, interference corrections and procedural blanks. Errors on total gas and error-weighted mean ages also include uncertainties in the *J* value (internal errors). Ar ages were calculated using the IUGS recommended constants (Steiger and Jäger, 1977).

## 4. Results

### *4.1. Description of LSU 1 lithostratigraphy*

We report here detailed lithostratigraphic descriptions of the three subunits of LSU 1 (Fielding et al., 2008b). In Figure 2 the stratigraphic section is shown. Brief interpretive summaries of paleoenvironmental conditions and modes of deposition for the sediments are given in this section followed by more thorough discussions in Section 5.

#### *4.1.1. Lithostratigraphic unit 1.1 (0–10.22 mbsf)*

Rocks recovered in the interval 0–9.02 mbsf are loose clasts (bagged samples) 2 to 9 cm in size. Among these, sample AND-2A 8.88a is a fresh subangular glomeroporphyritic lava clast of phonolite composition (Figure 5). It contains cm-sized anhedral anorthoclase phenocrysts (often with large glass inclusions), subhedral medium-grained phenocrysts of zoned clinopyroxene with pale-green augitic cores ($Wo_{46}$–$Fs_{17}$) and purple brown rims and minor olivine ($Fo_{52}$) set in an almost opaque glassy vesicular groundmass. Flattened vesicles and elongate phenocrysts define a flow texture. Another subangular lava clast, sample AND-2A 8.88b, is very similar in texture and mineral assemblage to sample AND-2A 8.88a but is trachytic in composition (Figure 5). Other clasts consist of scoriaceous basaltic lava with ~ 50% spherical vesicles and euhedral phenocrysts of clinopyroxene and elongate plagioclase (AND-2A 8.88c), and a clast of laminated hyaloclastite made up of very fine-grained light-brown fresh glass shards, angular sideromelane fragments with variable microlite compositions, sparse monomineralic clasts of euhedral olivine (≤ 500 μm), and minor opaque fragments (AND-2A 8.88d).

The interval between 9.02 and 9.86 mbsf comprises continuous core of laminated and ripple asymmetric cross-laminated volcanic sands that

**Table 2.** Modal data of sands and sandstones from LSU1 (500 clasts were counted per sample, values are percentages).

| | | | | | Q | | | F | | | | | | | | | |
|---|---|---|---|---|---|---|---|---|---|---|---|---|---|---|---|---|---|
| | | | | | Quartz | | | K-feldspar | | Plagioclase | | Other monomineralic phases | | | | | |
| Sample | | Grain-size sorting[a] (%) | matrix | crystal- | Mono-crystal-line | Poli-rock line | In silicic crystal-fragment | Mono-rock line | In silicic crystal-fragment | Mono-rock line | In silicic fragment | Pyroxene | Amphibole | Olivine | Biotite | Opaque | Zircon |
| AND-2A 9.34 | sand | vf-f | ws | - | 9.4 | 0.4 | 0.0 | 1.0 | 0.0 | 7.0 | 0.0 | 3.8 | 1.6 | 0.0 | 2.0 | 4.6 | 0.0 |
| AND-2A 9.61 | sand | f-m | ms | - | 6.6 | 0.2 | 0.0 | 2.4 | 0.0 | 5.4 | 0.0 | 1.8 | 0.4 | 1.8 | 0.4 | 2.2 | 0.0 |
| AND-2A 10.07 | sand | f-c | ms | - | 3.4 | 0.2 | 1.6 | 0.6 | 0.0 | 1.0 | 1.6 | 4.6 | 0.4 | 14.8 | 0.0 | 1.2 | 0.0 |
| AND-2A 22.81 | sandst. | f-m | ms | 15.7 | 6.4 | 0.0 | 0.0 | 0.0 | 0.0 | 9.8 | 0.0 | 1.8 | 1.8 | 0.0 | 0.4 | 2.2 | 0.0 |
| AND-2A 23.20 | sand | f-m | ws | - | 3.8 | 0.2 | 0.0 | 0.0 | 0.0 | 2.6 | 0.0 | 6.0 | 1.8 | 0.0 | 0.0 | 1.6 | 0.4 |
| AND-2A 23.62 | sand | m-c | ws | - | 3.6 | 0.6 | 0.0 | 0.2 | 0.0 | 2.0 | 0.0 | 7.4 | 0.8 | 0.0 | 0.0 | 0.8 | 0.0 |
| AND-2A 24.98 | sand | f-m | ws | - | 3.2 | 0.0 | 0.0 | 0.0 | 0.0 | 4.8 | 0.0 | 5.8 | 1.4 | 0.0 | 0.0 | 1.2 | 0.0 |
| AND-2A 25.81 | sand | f-m | ws | - | 8.0 | 0.8 | 0.0 | 2.2 | 0.0 | 8.8 | 0.2 | 3.4 | 2.8 | 0.0 | 0.0 | 2.4 | 0.0 |
| AND-2A 28.61 | sandst. | f-m | ws | 14.2 | 7.6 | 0.4 | 0.0 | 1.0 | 0.0 | 4.2 | 0.2 | 5.8 | 2.8 | 0.0 | 0.6 | 4.2 | 0.0 |
| AND-2A 30.42 | sand | m | ws | - | 1.8 | 0.2 | 0.0 | 0.0 | 0.0 | 2.6 | 0.0 | 2.2 | 0.8 | 0.0 | 0.0 | 5.4 | 0.0 |
| AND-2A 30.91 | sand | m | ws | - | 2.4 | 0.0 | 0.0 | 0.2 | 0.0 | 1.8 | 0.0 | 0.2 | 0.0 | 0.0 | 0.0 | 1.6 | 0.0 |

[a] ws: well sorted; ms: moderately sorted.

| | L | | | | | | | | | | | | | |
|---|---|---|---|---|---|---|---|---|---|---|---|---|---|---|
| | **Lv glassy** | | | | | | **Lv olocrystalline** | | | | | | | |
| | **Colorless glass (± micro-liths)** | **Light-brown glass shard** | **Light-brown sideromelane (± microliths and vesicles)** | **Dark-brown sideromelane (± microliths and vesicles)** | **Weathered sideromelane (± micro-liths)** | **Tachylite** | **Holo-crystalline volcanic rock (isotropic por-phyritic or equi-granular texture)** | **Holo-crystalline volcanic rock (trachytic texture)** | **Holo-crystalline volcanic rock (felsitic texture)** | **Medium -grade meta-morphic rock** | **Chert** | **Mudstone** | **Oolith** | **Opaque lithic clast** |
| AND-2A 9.34 | 0.0 | 10.4 | 30.0 | 0.0 | 14.6 | 7.2 | 3.4 | 0.0 | 0.0 | 0.0 | 0.0 | 2.0 | 1.0 | 1.6 |
| AND-2A 9.61 | 0.6 | 10.0 | 38.4 | 0.0 | 8.4 | 7.0 | 6.6 | 0.0 | 0.0 | 0.0 | 0.0 | 2.8 | 1.6 | 3.4 |
| AND-2A 10.07 | 0.0 | 6.4 | 38.0 | 0.0 | 12.2 | 7.6 | 1.0 | 1.6 | 0.0 | 0.0 | 0.0 | 1.4 | 0.0 | 2.4 |
| AND-2A 22.81 | 1.6 | 13.2 | 26.8 | 1.2 | 12.0 | 8.6 | 8.0 | 0.0 | 0.0 | 0.0 | 0.0 | 1.2 | 1.0 | 4.0 |
| AND-2A 23.20 | 1.0 | 0.0 | 24.0 | 1.0 | 27.6 | 8.2 | 15.6 | 0.0 | 0.0 | 0.0 | 2.0 | 2.4 | 0.0 | 1.8 |
| AND-2A 23.62 | 1.8 | 0.0 | 31.4 | 0.0 | 14.0 | 9.0 | 16.0 | 3.0 | 5.4 | 1.2 | 0.0 | 1.6 | 0.0 | 1.2 |
| AND-2A 24.98 | 1.4 | 0.0 | 43.2 | 0.0 | 17.4 | 3.0 | 13.0 | 1.2 | 0.6 | 0.8 | 1.2 | 0.4 | 0.6 | 0.8 |
| AND-2A 25.81 | 3.4 | 0.0 | 35.6 | 1.8 | 10.8 | 7.0 | 8.2 | 0.0 | 1.0 | 0.2 | 0.8 | 1.0 | 1.6 | 0.0 |
| AND-2A 28.61 | 6.6 | 0.0 | 30.6 | 0.8 | 11.6 | 14.4 | 6.8 | 0.0 | 0.0 | 0.0 | 0.4 | 2.0 | 0.0 | 0.0 |
| AND-2A 30.42 | 4.0 | 0.0 | 50.0 | 1.4 | 7.2 | 15.8 | 8.4 | 0.0 | 0.0 | 0.0 | 0.0 | 0.2 | 0.0 | 0.0 |
| AND-2A 30.91 | 0.4 | 0.0 | 75.6 | 1.8 | 2.6 | 9.4 | 0.8 | 0.0 | 0.0 | 0.0 | 0.2 | 1.6 | 1.4 | 0.0 |

[a] ws: well sorted; ms: moderately sorted.

are partly lithified (Figure 6). This interval is characterized by finer and more rounded fragments at the top. Component analyses of 2 samples (AND-2A 9.34 and 9.61) show that the overall composition is similar within the deposit and heterolithic (Figure 4). The main component are fresh, vesicular sideromelane clasts and minor angular to subangular glass shards and altered sideromelane, light-brown in color. The latter contains a variable amount of microlites and 10–50 micron-sized, round vesicles filled by clay (Figure 7a). Monomineralic felsic grains and holocrystalline lava clasts are also present, as well as rare ooliths (Figure 8a–d). The term oolith is used here to indicate a small rounded grain of sedimentary origin consisting of a concentrically layered coating around a nucleus, according to the definition of the AGI Glossary of Geology (Neuendorf et al., 2005; Flügel, 2004). The coating material is made of an aggregate of cryptocrystals (on average a few μm in size), and it is characterized optically by variable second-order birefringence colors. The largest crystals of the coating commonly exhibit an elongate shape. The long axes of these crystals are generally aligned to the surface of the nucleus, defining a tangential pattern in the coating. A silicatic (non-carbonate) composition for the coating is inferred on the basis of optical features and shape. The contact between core fragments (angular quartz, sideromelane, tachylite or lava) and their coatings is sharp (Figure 8).

The succession continues downward with full core recovery into a brown volcaniclastic gravel and sand layer showing a pebble-rich horizon at the contact with the overlying sands (interval 9.86–10.15 mbsf). These clasts are well-rounded and mainly composed of basaltic lava. Component analyses of the sandy fraction indicates a major contribution of fresh light-brown sideromelane grains often with olivine ($Fo_{83}$) and subordinate pyroxene crystals (occurring also as loose crystals up to 1 mm) and glass shards (Figure 4, sample AND-2A 10.07). Euhedral olivine is also found in altered sideromelane clasts that, along with tachylite clasts, constitute a significant fraction of the sand. Minor components are quartz and plagioclase found in granular holocrystalline rock fragments as well as rare monocrystalline perthitic K-feldspar up to 500 μm in size. This coarse-grained deposit presents features similar to those of the previous layer (9.02–9.86 mbsf), indicating an analogous process of sedimentation.

*4.1.2. Lithostratigraphic unit 1.2 (10.22–20.57 mbsf)*

Neither the upper nor the lower contact of LSU 1.2 is preserved due to poor recovery. In the continuous core of interval 10.22–10.44 mbsf, sub-rounded cm-sized basanite clasts were recovered. One of these, sample AND-2A 10.22 is a variably vesicular (5–20%) basanite lava clast characterized by a phenocryst assemblage of euhedral skeletal olivine up to 4 mm in length and minor clinopyroxene in a brown glassy groundmass with microlites of clinopyroxene, plagioclase and oxides. Vesicles are irregular in shape and the groundmass consists of patches and streaks of a black to almost opaque glass. This sample has been dated by the $^{40}Ar$–$^{39}Ar$ method with an age of 662 ± 42 ka (± 2σ internal error; Di Vincenzo et al., submitted).

The interval between 10.44 and 12.23 mbsf is a continuous core of a black volcanic monomictic clast-supported breccia composed of poorly sorted, highly angular to sub-angular cm-sized variably vesicular clasts and glassy micro-vesicular fragments (Figure 9), both containing phenocrysts of compositionally homogeneous euhedral to skeletal olivine ($Fo_{83–86}$, AND-2A 11.36). The lava clasts within the breccias are basanite in composition (Figure 5) and some of them show reddened, oxidized margins. This deposit also contains some lava clasts with different mineralogy and texture. For example, sample AND-2A 10.79 is a black, strongly vesicular basanite lava with an abundance of subspherical 1–2 mm vesicles (~ 50% by volume) filled by secondary calcite. This sample also contains euhedral mm-sized phenocrysts of olivine ($Fo_{86}$) and microphenocrysts of clinopyroxene ($Wo_{48}$–$Fs_{40}$), the latter also occurring as microlites in the groundmass. Another clast, AND-2A 11.94, contains abundant clinopyroxene phenocrysts and minor olivine microphenocrysts in a glassy groundmass with microlites of clinopyroxene and olivine as well as plagioclase and magnetite.

The lower portion of LSU 1.2, between 12.23 and 20.57 mbsf, is in bagged samples composed of subrounded variably vesicular basaltic lava clasts. Sample AND-2A 12.23 is a glomeroporphyritic vesicular hawaiite lava clast (Figure 5) characterized by phenocrysts of zoned clinopyroxene (pale-green core to purple brown rim) and minor olivine in a glassy groundmass that includes microlites of plagioclase, clinopyroxene and magnetite. The mm-sized subspherical vesicles are partially filled with secondary calcite. The hawaiite lava clast sample AND-2A 18.03 contains spherical vesicles and phenocrysts of zoned clinopyroxene and minor altered olivine in a glassy groundmass that includes microlites of clinopyroxene, plagioclase and oxides. Sample AND-2A 18.63 is a vesicular (20%) tephrite containing euhedral phenocrysts of zoned clinopyroxene, minor olivine and rare plagioclase microphenocrysts in a hypocrystalline groundmass made of a light brown interstitial glass with microlites of clinopyroxene, plagioclase and magnetite. Finally, sample AND-2A 18.69 presents clinopyroxene as phenocrysts and minor bowlingitic olivine and it is compositionally similar to the previous sample.

The nearly 2 meter thick interval of volcanic breccias near the top of LSU 1.2 is interpreted to represent a minimally reworked autoclastic breccias similar to what is formed by autobrecciation of a subaerially erupted lava (McPhie et al., 1993). Some lava blocks mainly at the base of the breccia show reddish scoriaceous edges, which typically indicate subaerial eruption and deposition. No genetic association between the breccia and underlying bagged lava clasts is implied, given the differences in their petrographic features and chemical compositions (Figure 5).

*4.1.3. Lithostratigraphic Unit 1.3 (20.57– 37.07 mbsf)*

Only bagged samples were recovered from the top of LSU 1.3 (20.57–21.96 mbsf) and they consist of fragments of black vesicular basalts and volcanic sandstone to claystone.

Continuous core recovery starts below 21.96 mbsf with a volcanic, yellowish, pebble-rich sandy siltstone containing subrounded muddy intraclasts and volcanic granules represented by both fresh and altered sideromelane, tachylite and minor lava clasts. Fragments of poly- and monocrystalline quartz, plagioclase and minor amphibole are also present (sample AND-2A 22.11). A weak stratification in the sandy siltstone is defined locally by clast concentrations and alignments.

The interval 22.44–22.76 mbsf is characterized by a volcanic breccia with a variable amount of sandy-muddy matrix. The intermediate part is enriched in sideromelane granules and minor black vesicular lava with euhedral plagioclase, clinopyroxene and olivine phenocrysts (AND-2A 22.60). The basal contact is irregular, apparently as a result of soft-sediment loading.

The succession continues downward into a 10 cm-thick volcaniclastic layer consisting exclusively of Y-shaped and angular 10–100 μm glass shards with subordinate clinopyroxene microlites (Figure 7b). This vitroclastic deposit is interlayered with a ~5 cm-thick moderately sorted fine- to medium-grained sandstone (AND-2A 22.81) composed of subrounded to angular sideromelane and tachylite clasts and broken crystal fragments in a siliciclastic matrix (~15%; Figure 4). The upper contact of this sandstone is represented by a ~30° dipping dark layer of irregular thickness (up to 2 mm thick) including both tiny angular glass shards from the vitroclastic deposit and medium sand-sized clasts (mostly sideromelane) in a dark interstitial cement of homogeneous siderite composition as indicated by microprobe data (Figure 7b). The glassy fragments of the sandstone are dominated by light brown sideromelane with a variable amount of vesicles and microlites, and subordinate colorless glassy fragments and dark-brown sideromelane. Altered sideromelane, tachylite, lava clasts and minor ooliths follow in order of abundance. Grains of quartz and plagioclase occur in addition to the lithic volcanic components.

A 10 cm-thick mudstone with dispersed black volcanic granules passes downward into a normally graded volcanic sandstone bed

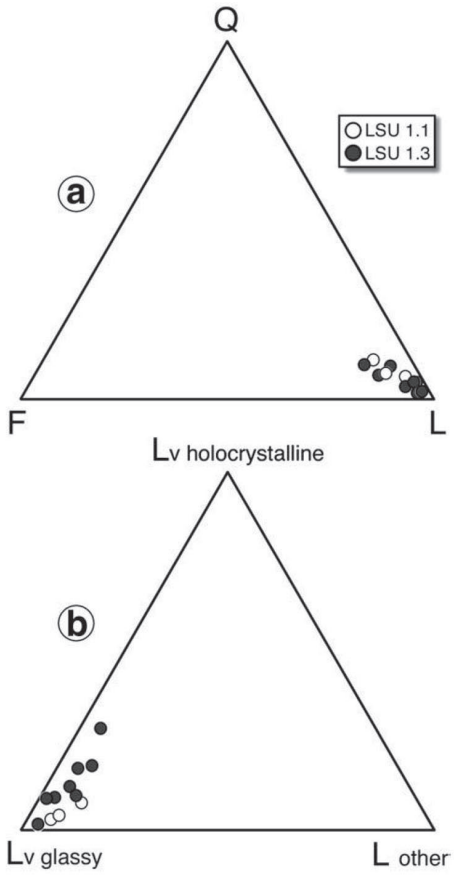


**Figure 3.** Modal compositional data of LSU 1 sand and sandstones plotted on: a) QFL diagram (Dickinson, 1985); b) ternary diagram where the end-member lithic volcanic (Lv) compositions are: Lv glassy, Lv holocrystaline and Lv other (see Table 2 for a comprehensive list of the rock types grouped into each end-member).

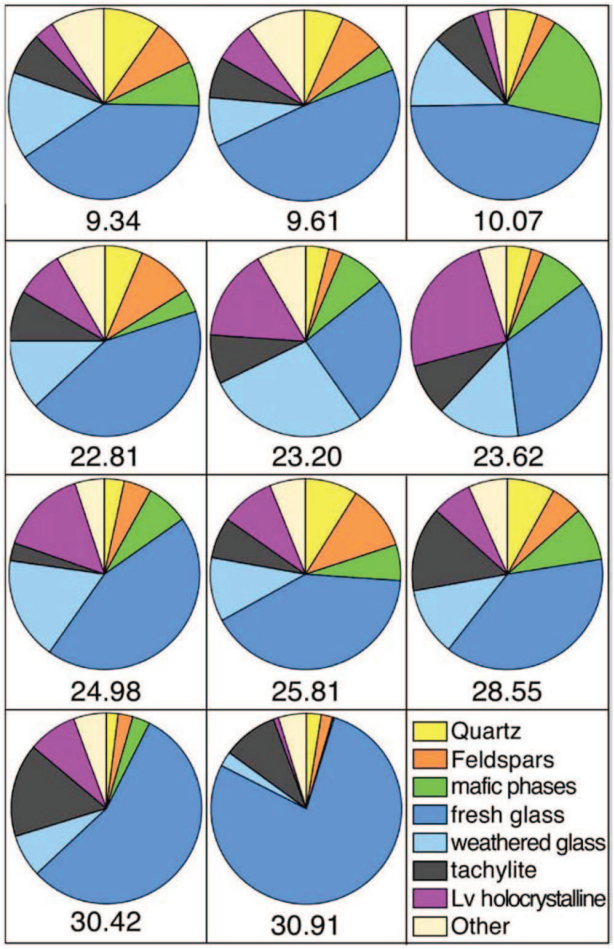


**Figure 4.** Pie-charts illustrating the modal composition of LSU 1 sands and sandstone. The most representative components are plotted.

(23.04–23.70 mbsf), which grades from red medium sand at the top to brownish black and coarse sand at the base. Altered and fresh sideromelane dominates among the volcanic components (sample AND-2A 23.20), followed by lava and tachylite clasts. Grains of monocrystalline quartz and plagioclase, as well as of pyroxene and subordinate amphibole, represent the other significant components in this rock (Figure 7c). Rare chert and rounded mudstone fragments also occur. The medium sand contains up to 1 cm-wide zones of red cemented sandstone, which presents the same subangular to subrounded clasts found in the sand (Figure 4). The cement is amorphous according to XRD data. Optical microscopy and SEM-EDS analyses reveal a two-stage cementation process (Figure 10). First, lobate pore lining domains composed of a mixture of FeO (up to 70%), $SiO_2$, $Al_2O_3$, with subordinate amounts of $TiO_2$, $P_2O_5$, CaO and $K_2O$ originally formed on grain surfaces. Afterwards they were overgrown by isopachous (~ 5 µm) Fe-dominated rims. Occasionally, a red cement with a composition analogous to that of the pore lining domains is also found as a thin coating or tiny spots on loose sand-sized clasts (Figure 10c and 10d, respectively). Sample AND-2A 23.62 is a well-sorted medium- to coarse-grained sand (Figure 7e) whose components are the same as sample AND-2A 23.20, with the addition of rare microcline and medium-grained sericitized plagioclase, polycrystalline quartz, and low- to medium-grade metamorphic rock fragments. The fragments of this sand are rounded to subrounded indicating a significant degree of reworking.

The non-stratified volcanic breccias to pebbly mudstones of the upper part of LSU 1.3 were most likely emplaced by debris flows or possibly the basal traction carpet of turbidity currents given their matrix supported and poorly sorted nature with soft sediment deformation at the base (e.g. Anderson et al., 1984). The normally graded, moderate to well-sorted sands were likely deposited by turbidity currents. The poorly-sorted, weakly stratified pebbly mudstones/sandstones may have been deposited from coarse debris melting out of surface ice and minimally transported by downslope currents. See discussions by Sohn (1997), Mutti et al. (1999), Shanmugam (2000, 2002), Mutti et al. (2003), and Mohrig and Marr (2003) when referring to debris flows, sandy debris flows, high-density turbidity current, hyperconcentrated flow, granular flow and flowslides.

A volcanic sandstone occurs from 24.90 to 25.27 mbsf following several meters of drilling with 0% core recovery. It is grayish-black, well-sorted, medium-grained, and stratified at mm- to cm-scale, with a sharp lower contact. It contains subrounded to subangular monomineralic and lithic clasts similar both in composition and relative abundances to the two samples from the overlying sandstone, including ooliths (Figure 8e, sample AND-2A 24.98). It is noteworthy that glassy fragments found within this interval are subrounded.

The succession continues downward with a series of cm-scale layers of volcanic sandstone, siltstone and mudstone with dispersed coarser clasts and a volcanic granule breccia (interval 25.27–25.93 mbsf). In this interval samples AND-2A 25.54 and 25.81 are a reddish fine sand and a medium sand, respectively, containing subrounded glassy granules (Figure 4) and rare fragments of a red cement similar (based on optical properties) to that found in sample AND-2A 23.20. Remarkably, sample AND-2A 25.81 contains ooliths with monocrystalline quartz or siderolemane nuclei (Figure 8f–g). Basal contacts of many of the coarser intervals are

**Table 3.** Whole rock major element composition (wt.%) of LSU1 lava clasts. DI: Juergens Island in Dailey Islands group. Errors are between 4–7%, 2–4% and about 1% respectively, for abundances ranging from 0 to 1%, 1 to 10% and 10 to 65%.

| Sample | AND-2A 8.88a | AND-2A 8.88b | AND-2A 8.88c | AND-2A 10.22 | AND-2A 10.79 | AND-2A 11.94 | AND-2A 12.23 | AND-2A 18.03 | AND-2A 18.63 | AND-2A 18.69 | AND-2A 27.39 | DI |
|---|---|---|---|---|---|---|---|---|---|---|---|---|
| LSU | LSU1.1 | LSU1.1 | LSU1.1 | LSU1.1 | LSU1.2 | LSU1.2 | LSU1.2 | LSU1.2 | LSU1.2 | LSU1.2 | LSU1.3 | 2007 |
| $SiO_2$ | 55.74 | 59.54 | 49.28 | 45.48 | 43.41 | 44.21 | 47.44 | 47.10 | 44.66 | 45.69 | 42.21 | 43.43 |
| $TiO_2$ | 0.97 | 0.86 | 2.86 | 3.07 | 3.08 | 3.05 | 2.89 | 3.17 | 3.31 | 3.17 | 3.93 | 3.21 |
| $Al_2O_3$ | 19.53 | 17.10 | 13.65 | 13.13 | 13.26 | 13.86 | 13.03 | 14.10 | 14.76 | 14.10 | 13.71 | 13.49 |
| $Fe_2O_{3tot}$ | 5.62 | 4.75 | 9.99 | 12.37 | 12.47 | 11.99 | 11.30 | 11.51 | 11.37 | 11.28 | 12.15 | 12.55 |
| MnO | 0.20 | 0.18 | 0.13 | 0.20 | 0.20 | 0.20 | 0.19 | 0.19 | 0.20 | 0.19 | 0.17 | 0.19 |
| MgO | 0.90 | 0.79 | 4.57 | 8.98 | 9.58 | 8.83 | 8.29 | 6.00 | 5.86 | 5.95 | 8.57 | 9.41 |
| CaO | 2.80 | 2.53 | 10.51 | 10.27 | 10.49 | 10.35 | 9.52 | 10.42 | 11.06 | 10.50 | 11.23 | 11.09 |
| $Na_2O$ | 7.89 | 6.93 | 3.13 | 3.92 | 3.68 | 4.30 | 4.00 | 4.42 | 4.59 | 4.45 | 3.37 | 3.83 |
| $K_2O$ | 4.45 | 4.00 | 1.12 | 1.75 | 1.74 | 1.92 | 1.79 | 1.93 | 2.04 | 1.91 | 1.93 | 1.66 |
| $P_2O_5$ | 0.35 | 0.30 | 0.49 | 0.72 | 0.70 | 0.74 | 0.67 | 0.71 | 0.79 | 0.72 | 0.91 | 0.61 |
| LOI | 1.38 | 2.04 | 4.35 | 0.46 | 1.29 | 1.09 | 0.70 | 1.30 | 1.09 | 0.73 | 2.13 | 0.14 |
| Total | 99.83 | 99.02 | 100.08 | 100.35 | 99.90 | 100.54 | 99.82 | 100.85 | 99.73 | 98.69 | 100.31 | 99.61 |

sharp and in some cases may be erosional. Most breccia units contain up to 1 cm-sized grains, with the coarsest grained interval containing cobble-sized clasts. These coarser-grained intervals are olive-grey to grayish-black in color, and in some cases are faintly stratified and coarsen upward.

Interval 25.93–26.28 mbsf is characterized by pale olive to olive gray volcanic siltstone and medium sandstone with dispersed clasts. The two lithologies are interlaminated to thinly interbedded, generally at scales < 1 cm. Analyses indicate a composition comparable to those of the overlying sand layers with fresh sideromelane glass being the prevailing clast type (Figure 4, samples AND-2A 25.95, 26.33).

Interbedded volcanic sandy breccia and volcanic sandy siltstone occur between 26.28 and 27.09 mbsf, the latter with abundant intraformational mudstone clasts. The sandy breccia forms 90% of this interval in cm-scale beds separated by laminations of siltstone. There is an overall coarsening upward trend from granule to pebble at the top.

Downcore, a 20 cm-thick asymmetric ripple cross-laminated fine-grained volcanic sandstone, sample AND-2A 27.19, is composed of sideromelane and lava clasts and crystals (7–16%). Ripple sets are < 1 cm thick.

Next is a sandy volcanic breccia containing scoria lapilli (interval 27.30–27.70 mbsf, AND-2A 27.65). An angular clast from the breccia (sample AND-2A 27.39) is a porphyritic lava, basanitic in composition (Figure 5), with normally- and reversely-zoned phenocrysts of clinopyroxene, minor bowlingitic olivine and a third phase that has been completely replaced by opaque minerals. The phenocrysts are set within a slightly hypocrystalline groundmass containing microlites of plagioclase, clinopyroxene and magnetite. The sandy breccia passes downward into a clast-supported pebble-breccia (interval 27.70–28.12 mbsf) with clasts dominated by intraformational compacted volcanic sediments.

Interval 28.12–28.39 mbsf is a volcanic fine to very fine sandstone bedded at mm-to cm-scale including hummocky cross stratification (Figure 11), asymmetrical trough cross-lamination, and a 1 cm-thick bioturbated layer. The hummocky cross-stratification is composed of dark grey to black thin beds to lamina. The black beds (sample AND-2A 28.21) are composed of tiny transparent glass shards. Beds/lamina of hummocks and swales cross-cut each other in erosive contact, and dip in opposing directions at ~10–15 degrees.

The core continues with a well sorted fine- to medium-grained vol-

**Table 4.** Representative electron microprobe glass analyses of major element (wt.%). 22.81 h: hyaloclastite layer. Relative error: $SiO_2$ 0.80%, $TiO_2$ 3.35%, $Al_2O_3$ 0.75%, $Fe_2O_{3tot}$ 1.37%, MnO 17.70%, CaO 1.20%, $Na_2O$ 1.6%, $K_2O$ 1.35%, $P_2O_5$ 6.03%.

| Sample AND-2A | 9.34 | 9.34 | 9.61 | 9.61 | 10.07 | 10.07 | 11.36 | 11.36 | 22.6 | 22.6 | 22.81 | 22.81 h |
|---|---|---|---|---|---|---|---|---|---|---|---|---|
| $SiO_2$ | 43.66 | 44.25 | 45.27 | 55.01 | 44.98 | 44.80 | 43.22 | 44.97 | 48.02 | 43.71 | 44.16 | 45.24 |
| $TiO_2$ | 3.72 | 3.45 | 3.12 | 1.33 | 3.10 | 3.36 | 3.64 | 2.90 | 3.01 | 3.78 | 4.02 | 3.41 |
| $Al_2O_3$ | 14.95 | 16.10 | 15.37 | 18.71 | 14.97 | 14.97 | 16.32 | 17.44 | 17.36 | 15.04 | 14.66 | 16.35 |
| $Fe_2O_{3tot}$ | 11.38 | 11.24 | 11.88 | 5.85 | 11.72 | 12.00 | 11.45 | 12.41 | 9.15 | 10.28 | 10.30 | 11.19 |
| MnO | 0.18 | 0.20 | 0.23 | 0.23 | 0.16 | 0.14 | 0.28 | 0.26 | 0.22 | 0.16 | 0.19 | 0.17 |
| MgO | 5.66 | 4.42 | 5.68 | 1.03 | 6.49 | 6.40 | 4.43 | 2.75 | 3.47 | 5.82 | 5.74 | 4.20 |
| CaO | 12.19 | 9.74 | 11.88 | 2.48 | 11.99 | 11.93 | 10.84 | 8.02 | 8.39 | 13.00 | 13.02 | 10.33 |
| $Na_2O$ | 4.52 | 5.03 | 3.94 | 7.68 | 3.45 | 3.44 | 5.56 | 6.42 | 5.99 | 4.49 | 4.53 | 5.22 |
| $K_2O$ | 1.82 | 2.17 | 1.19 | 5.55 | 0.89 | 0.89 | 2.25 | 2.75 | 2.66 | 1.87 | 1.80 | 2.20 |
| $P_2O_5$ | 0.79 | 0.95 | 0.53 | 0.34 | 0.37 | 0.39 | 1.09 | 1.32 | 0.88 | 0.83 | 0.80 | 0.94 |
| Total | 99.02 | 97.63 | 99.17 | 98.27 | 98.17 | 98.44 | 99.35 | 99.42 | 99.31 | 99.09 | 99.30 | 99.35 |
| Sample AND-2A | 23.2 | 23.2 | 23.62 | 23.62 | 25.54 | 25.54 | 27.19 | 27.19 | 30.42 | 30.42 | 30.91 | 30.91 |
| $SiO_2$ | 43.56 | 44.28 | 45.83 | 43.14 | 45.04 | 45.32 | 47.10 | 52.81 | 50.38 | 44.60 | 46.56 | 46.07 |
| $TiO_2$ | 4.07 | 6.20 | 3.06 | 3.98 | 3.64 | 3.86 | 3.33 | 1.99 | 2.06 | 3.54 | 3.70 | 3.82 |
| $Al_2O_3$ | 14.56 | 13.85 | 16.49 | 15.57 | 16.05 | 16.06 | 15.55 | 17.06 | 17.94 | 16.04 | 16.54 | 16.35 |
| $Fe_2O_{3tot}$ | 10.67 | 13.49 | 11.06 | 11.95 | 11.21 | 11.00 | 10.03 | 7.96 | 8.88 | 11.16 | 9.63 | 10.06 |
| MnO | 0.15 | 0.18 | 0.25 | 0.16 | 0.22 | 0.20 | 0.23 | 0.30 | 0.31 | 0.26 | 0.17 | 0.20 |
| MgO | 6.04 | 4.97 | 4.03 | 5.45 | 4.18 | 4.16 | 5.31 | 2.56 | 2.09 | 4.72 | 4.14 | 4.00 |
| CaO | 13.23 | 10.56 | 9.47 | 12.08 | 10.30 | 10.19 | 10.75 | 5.27 | 6.86 | 9.48 | 9.18 | 8.72 |
| $Na_2O$ | 3.94 | 3.05 | 5.65 | 4.61 | 5.33 | 5.22 | 4.49 | 6.45 | 6.26 | 4.60 | 5.46 | 5.35 |
| $K_2O$ | 1.61 | 1.71 | 2.42 | 1.95 | 2.28 | 2.32 | 1.89 | 3.62 | 3.08 | 2.22 | 2.54 | 2.56 |
| $P_2O_5$ | 0.73 | 1.13 | 1.12 | 0.82 | 1.15 | 1.08 | 0.81 | 0.82 | 0.94 | 1.29 | 0.79 | 0.99 |
| Total | 98.64 | 99.62 | 99.55 | 99.74 | 99.56 | 99.56 | 99.54 | 98.95 | 98.91 | 98.04 | 98.85 | 98.25 |

**Table 5.** Laser step-heating $^{40}Ar$–$^{39}Ar$ data. Argon isotope concentrations are $\times 10^{-15}$ mol. Data corrected for post-irradiation decay, mass discrimination effects, isotopes derived from interference reactions and blanks.

| No. | Laser power (W) | $^{36}Ar_{(atm)}$ | $^{37}Ar_{(Ca)}$ | $^{38}Ar_{(Cl)}$ | $^{39}Ar_{(K)}$ | $^{40}Ar_{(Tot)}$ | Age(Ma) | ± 2σ | $^{40}Ar$% | $^{39}Ar_K$% | Ca/K | ± 2σ |
|---|---|---|---|---|---|---|---|---|---|---|---|---|
| *Dailey Island, groundmass, grain size 0.30–0.50 mm, 52.6 mg, irradiation PAV-65, J = 0.0001875 ± 0.0000010* | | | | | | | | | | | | |
| 1 | 0.20 | 0.08510 | 0.1952 | 0.00220 | 0.3238 | 27.14 | 2.1 | 1.1 | 7.4 | 1.1 | 1.14 | 0.18 |
| 2 | 0.50 | 0.2123 | 3.308 | bdl | 10.02 | 88.74 | 0.878 | 0.053 | 29.3 | 35.6 | 0.623 | 0.038 |
| 3[a] | 0.70 | 0.05761 | 2.963 | 0.00455 | 5.419 | 29.87 | 0.802 | 0.051 | 42.9 | 19.2 | 1.032 | 0.061 |
| 4[a] | 0.90 | 0.03461 | 2.319 | 0.00648 | 3.713 | 18.86 | 0.786 | 0.065 | 45.7 | 13.2 | 1.178 | 0.070 |
| 5[a] | 1.2 | 0.03324 | 1.830 | 0.00675 | 3.185 | 16.79 | 0.739 | 0.078 | 41.4 | 11.3 | 1.084 | 0.064 |
| 6 | 1.5 | 0.03988 | 1.989 | 0.00853 | 2.368 | 16.56 | 0.682 | 0.049 | 28.8 | 8.4 | 1.585 | 0.094 |
| 7 | 1.9 | 0.04655 | 11.14 | 0.01055 | 2.150 | 18.04 | 0.674 | 0.061 | 23.7 | 7.6 | 9.77 | 0.56 |
| 8 | 2.5 | 0.01898 | 14.91 | 0.00433 | 0.6840 | 6.643 | 0.51 | 0.21 | 15.5 | 2.4 | 41.1 | 2.4 |
| 9 | 6.0 | 0.01123 | 18.91 | 0.00316 | 0.1677 | 3.501 | 0.37 | 0.83 | 5.2 | 0.6 | 213 | 14 |
| 10 | 15 | 0.01173 | 31.88 | 0.00338 | 0.1514 | 3.627 | 0.4 | 1.3 | 4.4 | 0.5 | 397 | 29 |
| Total gas age | | | | | | | 0.802 | 0.030 | | | | |
| Error-weighted mean age, MSWD = 0.90 | | | | | | | 0.784 | 0.036 | | 43.7 | | |
| *Dailey Island, replicate, groundmass, grain size 0.30–0.50 mm, 41.2 mg, irradiation PAV–65, J = 0.0001875 ± 0.0000010* | | | | | | | | | | | | |
| 1 | 0.15 | 0.03429 | 0.06539 | 0.00145 | 0.08169 | 10.75 | 2.5 | 1.6 | 5.7 | 0.5 | 1.51 | 0.19 |
| 2 | 0.30 | 0.1040 | 0.6284 | 0.00081 | 1.743 | 35.57 | 0.94 | 0.10 | 13.6 | 10.3 | 0.680 | 0.043 |
| 3[a] | 0.45 | 0.05098 | 1.297 | bdl | 3.963 | 24.39 | 0.796 | 0.035 | 38.2 | 23.5 | 0.618 | 0.037 |
| 4[a] | 0.60 | 0.03235 | 1.669 | 0.00175 | 3.186 | 16.70 | 0.758 | 0.042 | 42.7 | 18.9 | 0.989 | 0.058 |
| 5[a] | 0.80 | 0.01727 | 1.310 | 0.00365 | 2.085 | 9.870 | 0.773 | 0.064 | 48.2 | 12.3 | 1.186 | 0.070 |
| 6[a] | 1.1 | 0.01669 | 1.240 | 0.00491 | 2.100 | 9.650 | 0.760 | 0.047 | 48.8 | 12.4 | 1.114 | 0.065 |
| 7 | 1.4 | 0.02765 | 1.688 | 0.00512 | 1.790 | 11.64 | 0.66 | 0.10 | 29.8 | 10.6 | 1.78 | 0.11 |
| 8 | 1.8 | 0.02447 | 4.846 | 0.00615 | 1.168 | 9.506 | 0.66 | 0.14 | 23.9 | 6.9 | 7.83 | 0.46 |
| 9 | 2.5 | 0.00960 | 6.152 | 0.00133 | 0.4342 | 3.596 | 0.59 | 0.30 | 21.1 | 2.6 | 26.7 | 1.6 |
| 10 | 6.0 | 0.01194 | 16.82 | 0.00264 | 0.2202 | 3.939 | 0.63 | 0.75 | 10.4 | 1.3 | 144.1 | 8.8 |
| 11 | 15 | 0.00888 | 25.10 | 0.00324 | 0.1261 | 2.844 | 0.6 | 1.8 | 7.7 | 0.7 | 375 | 25 |
| Total gas age | | | | | | | 0.771 | 0.031 | | | | |
| Error-weighted mean age, MSWD = 0.84 | | | | | | | 0.775 | 0.022 | | 67.1 | | |

a. Data used in the error-weighted mean calculation. Errors on step ages are analytical errors, including in run statistics and uncertainties in the discrimination factor, interference corrections and procedural blanks. Errors on total gas and error-weighted mean ages also include uncertainties in the *J* value. bdl: below detection limit.

canic sandstone (AND-2A 28.55) yellowish and reddish in the upper 20 cm, dark brownish grey in the remainder. The subrounded and compositionally heterogeneous grains are dominated by transparent glassy fragments of white and pale yellow color (Figure 5). Ooliths with cores of lava, quartz and sideromelane fragments occur as a minor component.

In summary, the upper middle part of LSU 1.3 contains poorly-sorted sandy breccias or muddy sandstones, often in coarsening upward sequences, alternating with rippled sands and hummocky cross-stratifi-

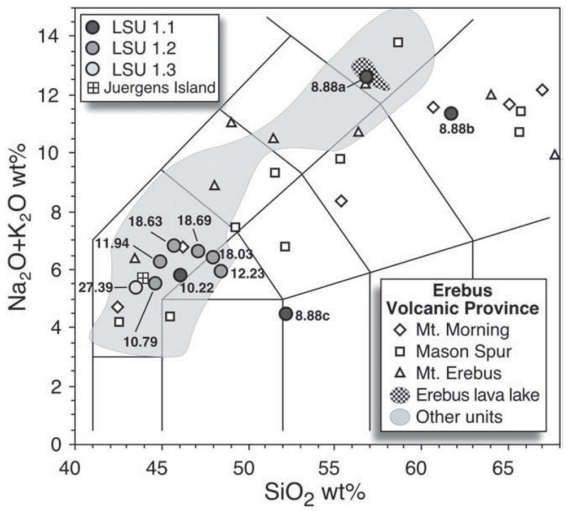


**Figure 5.** Whole rock composition of LSU 1 lava clasts plotted on the Total Alkali versus Silica diagram (Le Bas et al., 1986). Samples from this work are labeled according to the sampling level in the AND-2A core (mbsf). The composition of volcanic rocks from the Erebus Volcanic Province is plotted for comparison. Other units (46 samples) are: Franklin Island, Beaufort Island, Mount Bird, Mount Terror, Hut Point Peninsula, White Island, Black Island, Brown Peninsula, Minna Bluff, Mount Discovery, Royal Society Range, Taylor and Wright Valleys. Phonolite lava lake on Mount Erebus consists of 12 samples. Data from LeMasurier and Thomson (1990) and references therein, Kelly et al. (2008), Panter, unpublished data.

**Figure 6.** Photograph of ripple cross-laminated volcanic sands in the interval 9.02–9.86 mbsf.

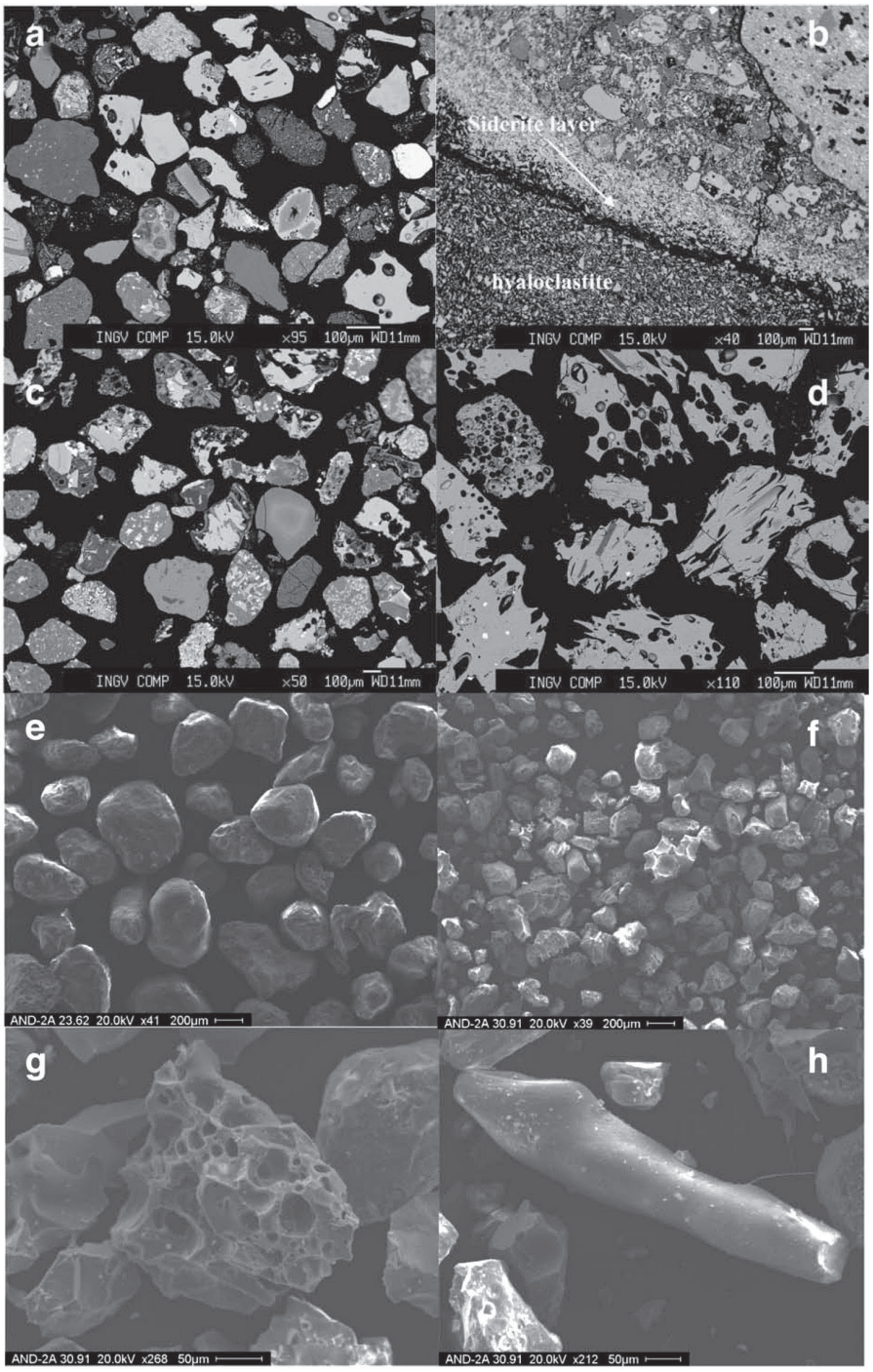


**Figure 7.** From a to d back scattered electron (BSE) images showing components of: (a) sample AND-2A 9.34; (b) sample AND-2A 22.81 (c) sample AND-2A 23.20; (d) sample AND-2A 30.91. From e to h SEM images of (e) sample AND-2A 23.82; (f) sample AND-2A 30.91; (g) vesicular sideromelane clast in sample AND-2A 30.91; (h) Pele's hair fragment in sample AND-2A 30.91.

cation. The hummocky cross-stratification is interpreted as deposited by oscillatory wave action, possibly combined with down slope turbidity current flow, based on the erosive contacts between hummocks and swales (e.g. Myrow et al., 2002, 2008; Lamb et al., 2008; Mulder et al., 2009). Ooliths indicate shallow water derivation for some of the sediments.

A medium-grained volcanic sandstone was recovered as bagged material from the interval 28.75–28.92 mbsf. This is followed by a coring gap of almost 1 m before more bagged material was recovered from the underlying interval at 29.56–30.18 mbsf. This contains a sandy volcanic breccia with polymict clasts, including volcanic rocks and pale grey sediment clasts.

A normally graded, olive grey to black, volcanic sandstone bed is present between 30.18 and 30.69 mbsf. The base of the deposit is characterized by pebble- to cobble-sized intraformational clasts of volcanic siltstone. Sample AND-2A 30.42 is dominated by glassy fragments with minor amounts of crystalline volcanic clasts (Figure 4).

Two fine-grained volcanic sandstone units occur at 30.69–30.86 mbsf and 30.86–31.27 mbsf. The upper sandstone is olive grey, normally graded with sparse laminae of grey medium-grained siltstone, and synsedimentary microfaults near the top and soft sediment deformation at the bottom. The lower sandstone unit is brownish-black with sparse laminae of medium grained volcanic sand. Sample AND-

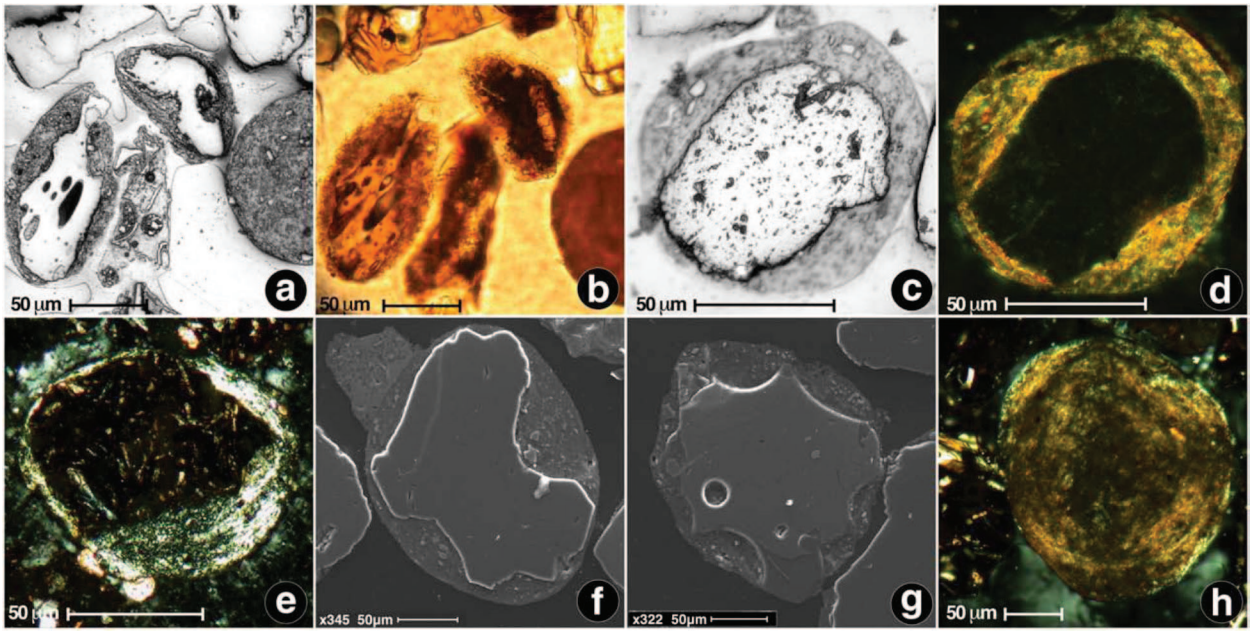


**Figure 8.** Photomicrographs of ooliths from LSU 1 with a nucleus of: a) two angular vesicular sideromelane fragments (sample AND-2A 9.34, left and top-center of picture), plane polarized reflected light (PPRL); b) same as previous, plane polarized light (PPL); c) a subangular glassy fragment (sample AND-2A 9.61), PPRL; d) same as previous, crossed polarized light (CPL); e) a tachylite clast (sample AND-2A 24.98), CPL; (f) an angular quartz fragment, (sample AND-2A 25.81), BSE image; g) a sideromelane grain, (sample AND-2A 25.81) BSE image. h) Oolith in which a nucleus is not visible, CPL. Note: i) the concentric pattern of the oolith coatings (d, e, h); ii) vesicle walls and convex shapes preserved in ooliths with glassy cores (a, g), ruling out a prolongate transport of these fragments from their place of origin to the shallow water environment where the ooliths formed.

2A 30.91 from the lower sandstone is almost completely (75%) composed of well vesicular, transparent sideromelane clasts with microlites of clinopyroxene and plagioclase, and Pele's hair (Figure 4; Figure 7d & 7f–h). This sample also contains ooliths with cores of lava, quartz and sideromelane fragments.

In summary, the lower middle part of LSU 1.3 contains both sandy breccia, probably deposited by debris flow, and fining up rippled sand layers, some with soft sediment deformation. These were most likely deposited as turbidites. Again, volcanic glass indicates variable reworking and the presence of ooliths indicates derivation from a shallow water source.

There is a coring gap of almost 4 m until the recovery of a unit of asymmetrically rippled, olive grey, volcanic fine sandstone with dispersed granules from interval 34.88–35.07. Ripples occur in 2–3 cm thick sets and microfaulting is present. This is followed by a muddy fine volcanic sandstone coarsening up to dispersed granules and pebbles at the top.

There is another gap of several meters filled by bagged material of volcanic fine sandstone. A grey massive sandstone occurs near the base of LSU 1.3 (36.34 mbsf). The components of this sandstone are dominated by basaltic glass (AND-2A 36.32) in the form of cuspate shards (< 0.1 mm) and vesicular sideromelane grains that vary from fresh to altered (palagonitized). Lithic clasts are scoria with plagioclase crystals and large vesicles. Probable volcanic-derived crystals include euhedral plagioclase, olivine, clinopyroxene and amphibole. Minor quartz along with trace amounts of biotite, chlorite, muscovite and a single granitoid lithic are present.

The succession continues downward with a black and whitish fine-grained, asymmetric ripple cross-laminated sandstone unit (36.38–36.85 mbsf). Sediments are almost entirely composed of tiny transparent dense fragments of glass with angular shapes (shards-bubble walls: sample AND-2A 36.62; Figure 12). The sandstone is underlain by a volcanic fine sandy mudstone with dispersed clasts with crude planar lamination at mm-scale. It is locally bioturbated, possibly by *Planolites,* indicating that the local environment was relatively clear water and not sediment clogged.

Underlying this is another rippled volcanic fine sandstone (AND-2A 37.07) in sharp contact with the underlying clast-rich, sandy diamictite of LSU 2 at 37.07 mbsf. The latter is the uppermost diamictite encountered in the core.

The basal part of LSU 1.3 is dominated by asymmetric rippled volcanic sandstones. These are again mainly composed of relatively fresh glass shards of near primary source deposited by turbidity currents.

### *4.2. Volcanic rock and glass chemistry*

Most of the lava clasts from LSU 1 are mafic and silica-undersaturated (normative nepheline, *ne* = 7–16 wt.%, Table 3). Whole rock compositions vary from basanite (AND-2A 10.22) to tephrite and hawaiite and form a broad cluster on the total alkali versus silica plot (Figure 5). This clustering suggests that, despite the differences in textures and ages (see below), the lava clasts were derived from genetically related magmas that are comparable to other mafic lavas within the Erebus Volcanic Province. It is worth noting that these mafic clasts show a variable affinity, ranging from moderately alkaline to strongly alkaline (Figure 5).

The first material recovered by drilling comprised unconsolidated sediments (bagged samples), including three lava clasts whose mineralogic assemblages and compositions differ significantly from each other. Samples AND-2A 8.88a and AND-2A 8.88b include large anorthoclase feldspar containing abundant glass inclusions. The clasts have evolved alkaline compositions and are classified as *ne*-normative (16 wt.%) phonolite and a *ne*-normative (12 wt.%) trachyte (Table 3, Figure 5). Sample AND-2A 8.88c is a subalkaline basalt/basaltic andesite, which is a distinctive composition relative to all other clasts that were analyzed from LSU 1.

Samples 8.88a and 8.88b are comparable to the known compositions from Mt. Erebus and also with other evolved volcanoes to the south (Mason Spur and proto-Mt. Morning) whereas sample 8.88c is unlike any other composition from the Erebus Volcanic Province, and might represent a product of Jurassic Ferrar subalkaline volcanism (Elliot et al., 1999). Compositional diversity of clasts in these unconsoli-

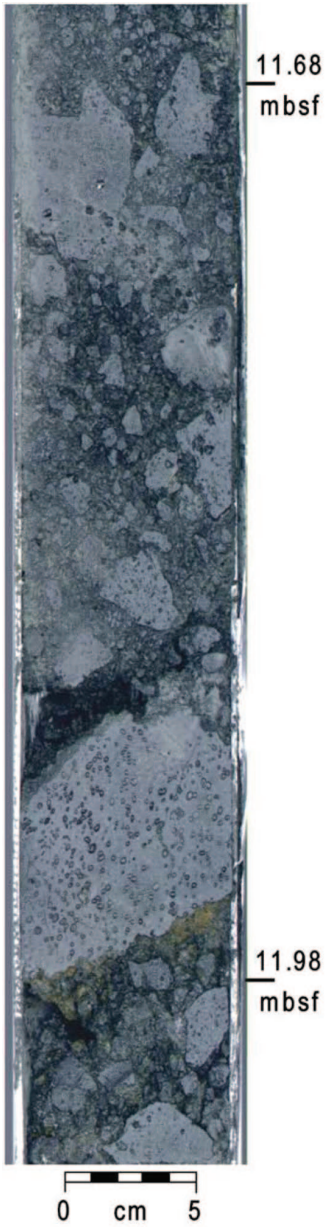


**Figure 9.** Photograph of black monomictic volcanic breccia (interval 11.65–12.04 mbsf), clast-supported, composed of angular and sub-angular cm-sized vesicular lava clasts and glassy micro-vesicular fragments.

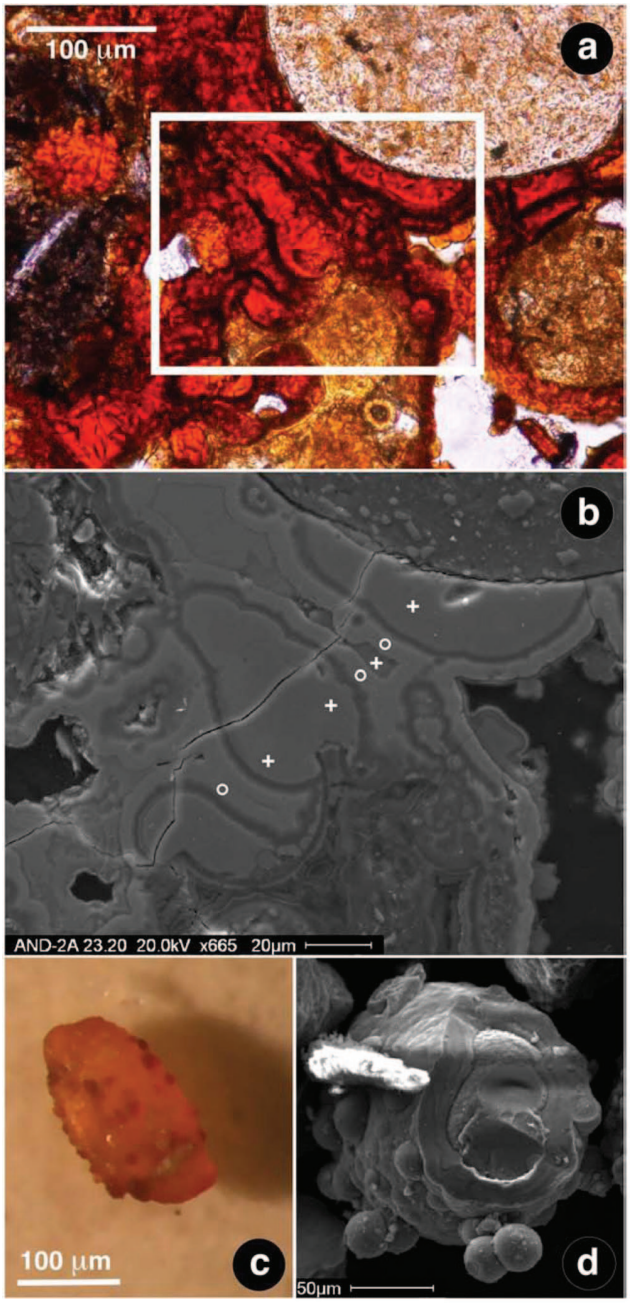


**Figure 10.** Sample AND-2A 23.30. a) Photomicrograph of the red cement partially consolidating the volcanic sand, PPL; b) detail of the white-framed inset of a), BSE image, showing the lobate pore filling domains (crosses) composed of FeO 50–70%, $SiO_2$ 15–30%, $Al_2O_3$ 5–10% and $TiO_2$ 2–5%, with a subordinate content of $P_2O_5$, CaO and $K_2O$ 1–3%, overgrown by isopachous (~ 5 μm) rims (circles) whose composition is dominated by FeO ~ 90%, with subordinate $SiO_2$ up to 10% and minor $Al_2O_3$ 1–2%; c) photograph of a quartz grain spotted with the red cement; d) loose sand clast coated with a cement analogous in composition to that of the pore filling domains (crosses of b), BSE image.

dated bagged samples from the top of the drill hole supports their recent deposition on the modern day seafloor by glacial drift; they are therefore not part of LSU 1 volcanoclastic sequence.

Glass fragments represent the most abundant component in the LSU 1 sediments. Glass occurs in a variety of types from transparent to colored sideromelane with or without crystals to tachylite, and also shows a wide range in vesicularity from dense shards to frothy fragments (40–70% vesicles by volume). We selected a wide spectrum of glass types for analysis and discarded altered fragments. Table 4 summarizes the major element composition of representative glass from LSU 1. The sums of the oxides are high (97–99 wt.%) indicating that the glass has not been significantly hydrated.

Compositions of LSU 1.1 glass range from alkali basalt to tephrite (Figure 13a ). The glass in each sample is not homogeneous, indicating that it was not produced by a single eruptive pulse. However, because each sample has the same overall range in composition it is likely that they represent mixtures from the same sources. Glass compositions in sample AND-2A 11.36 from the volcanic breccia in LSU 1.2 are homogeneous falling in the tephrite field, and show a slightly higher alkali content with respect to the other analyzed samples (Figure 13a). Also, most of the volcanic sediments in LSU 1.3 also show heterogeneous glass compositions for individual samples, ranging from tephrite to tephriphonolite. However, three samples collected from separate deposits of volcanic sand (AND-2A 22.81 hyaloclastite, AND-2A 25.54 and AND-2A 30.91) display homogeneous tephrite compositions (Figure 13b and c).

**Figure 11.** Photograph of bedded at mm-to cm-scale volcanic fine to very fine sandstone (interval 28.12–28.39 mbsf) including possible hummocky cross stratification and a 1 cm-thick bioturbated layer. In this interval the black beds are composed of tiny transparent glass shards. Arrows indicate low angle, cross-cutting contacts indicative of erosion in classic oscillatory flow producing hummocky cross-stratification.

### *4.3. Dailey Islands*

A lava flow sample was collected for this study from the steep southeastern slope of Juergens Island (77°53'06"S, 165°01'58.8"E, at about 70 m asl) to compare with LSU 1 as a potential source for the clasts. The sample is a black vesicular lava with ~ 20 vol.% phenocrysts of euhedral skeletal olivine and zoned clinopyroxene (pale core grading to brown rim). The groundmass is holocrystalline and made of clinopyroxene and plagioclase microlites, abundant euhedral magnetite and minor olivine. This lava is a *ne*-normative (15 wt.%) basanite (Table 3) and is comparable to the most basic lava clasts and glass found in LSU 1, as well as other mafic compositions of the Erebus Volcanic Province (Figure 5).

Groundmass separated from this sample was dated by the $^{40}Ar$–$^{39}Ar$ laser step-heating technique. The results are listed in Table 5 and presented as age spectra in Figure 14. A first run on a few tens of milligrams of sample-separate gave a discordant age profile, with a descending shape. Three consecutive steps from the intermediate temperature region and representing ~ 44% of the total $^{39}Ar_K$ released, define a concordant segment (MSWD = 0.90) yielding an error-weighted mean age of 784 ± 36 ka, overlapping within error with the total gas age (802 ± 30 ka). A second step-heating run was performed on the same groundmass separate using a higher-resolution heating schedule, in order to better resolve the concordant segment. In the replicate analysis, the concordant segment is defined by four consecutive steps, representing ~ 67% of the total $^{39}Ar_K$ released and yielding an error-weighted mean age of 775 ± 22 ka (Figure 14). The 775 ± 22 ka age, which is taken as the best estimate for the time of extrusion of the studied sample, is in excellent agreement with the age obtained by Tauxe et al. (2004) and also compares with those obtained for two volcanic clasts from LSU 1 from the 10.22–12.41 interval (Di Vincenzo et al., submitted).

## 5. Local paleogeography–paleoenvironment

Paleoenvironmental reconstructions in the southwestern Ross Sea area and their link with both the tectonic evolution of the southern Victoria Land Basin and recent volcanic activity are discussed in the light of the results presented. The composition of the volcaniclastic materials is used to draw indications about the nature of the volcanic source and its possible location with respect to the basin. The most significant results and the implications discussed in this section are summarized

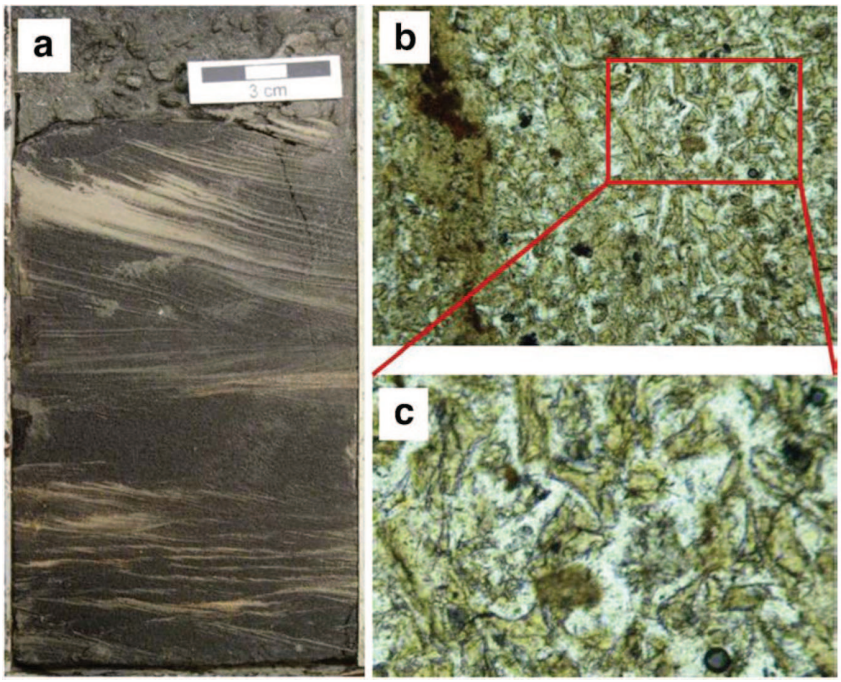


**Figure 12.** a) Photograph of ripple cross-laminated volcanic sands from interval 36.32–36.85 mbsf composed almost entirely of volcanic glass shards; b) photomicrograph of sample AND2-2A 36.32 at 10× magnification, field of view 2 mm; c) magnification of b) showing the cuspate Y-shape of the glass shards.

in Figure 15 as a sketch block diagram and a composite cartoon which illustrates the overall paleoenvironmental and tectonic setting inferred from the sedimentation interval of AND-2A LSU 1.

### *5.1. Evidence for local volcanic sources*

The sand-sized deposits of the LSU 1 are dominated by lithic components as shown in the QFL diagram (Dickinson, 1985; Figure 3a) and all samples plot in the litharenite field according to the sandstone classification by Pettijohn et al. (1987). The volcanic components within each sample are dominated by lithic fragments (Table 2), with glassy fragments the most abundant (Lv glassy, Figure 3b). Volcanic lithics also include holocrystalline lava clasts. Amphibole, pyroxene and olivine, the main mafic phases, occur as loose single crystal grains as well as phenocrysts in lava clasts within the same sample (e.g. sample AND-2A 10.07). Loose single crystals of plagioclase in many cases have similar textural and optical characteristics as coexisting plagioclase phenocrysts present in lava clasts, indicating the same or similar intrabasinal volcanic sources.

With the exception of LSU 1, all other lithostratigraphic units of the AND-2A core show a greater variety of volcanic compositions and basement lithologies (Panter et al., 2008).

Non-volcanic components occur throughout LSU 1 in minor amounts. The quartz (mostly monocrystalline, rarely polycrystalline), some of the plagioclase and rare K-feldspar are likely derived from granitoid sources, and hence are probably extrabasinal in origin. Low- and medium-grade metamorphic rock fragments (along with trace amounts of biotite, chlorite, and muscovite) are rare, with the exception of sample AND-2A 23.62, in which the contribution from a crystalline basement is larger. The overall scarcity of extrabasinal terrigenous detritus, in both the sandy fraction and large clasts, indicate that LSU 1 sediments mainly derive from the Cenozoic volcanic activity within the southern Victoria Land basin rather than from erosion of the Transantarctic Mountains. The paucity of extrabasinal sediments suggests a significant decrease in extrabasinal erosional activity in the area during the middle-late Pleistocene, perhaps because the area was covered by glaciers frozen to their base (Figure 15).

A significant amount of aeolian sediment deposited on the sea-ice around the drill-site has been documented by Atkins and Dunbar (2009) and consists of clay-sized to very coarse sand-sized particles that include highly angular volcanic grains, as well as well-rounded quartz grains. Larger clasts, including lava blocks, are present in areas of dirty ice on the McMurdo Ice Shelf (Figure 1b). In accordance with the findings of Atkins and Dunbar (2009), some of the quartz grains and other fine-grained non-volcanic components in LSU 1 might be from aeolian sediments originally deposited on sea ice.

On the basis of petrochemical analyses, most of the volcanic materials have mafic alkaline compositions ranging from basanite–tephrite to hawaiite, except the lava clasts in the topmost bagged samples, which are more evolved (phonolite and trachyte). All the analyzed materials from LSU 1, with the exception of one sample AND-2A 8.88c. fall within the compositional field of the Erebus Volcanic Province (Figure 5 and Figure 13), indicating their source from volcanic centers of the McMurdo Sound area.

To constrain the age of LSU 1, groundmass separates from two mafic lava samples (10.22–10.44 and 12.23–12.41 mbsf) were analyzed by the $^{40}Ar$–$^{39}Ar$ laser step-heating technique (Di Vincenzo et al., submitted) yielding a plateau age of 692 ± 38 ka and a mini-plateau age of 793 ± 63 ka (± 2σ internal errors), respectively. Results therefore suggest that the LSU 1, at least down to ~ 12.4 mbsf and possibly to ~ 16 mbsf, is younger than 1 Ma. Di Vincenzo et al. (submitted) also report much older total fusion ages of ~ 16.1 to ~ 9.5 Ma for mafic lava clasts from the 18.03–18.25 and 18.69–18.73-mbsf intervals, respectively. In light of possible provenance (Di Vincenzo et al., submitted), these data suggest that older clasts were transported and reworked before final deposition.

Volcanic deposits of similar age and composition to LSU 1 are found as cinder cones and lava flows scattered throughout the Erebus Volcanic Province (Kyle, 1990; Lawrence et al., 2009], and references

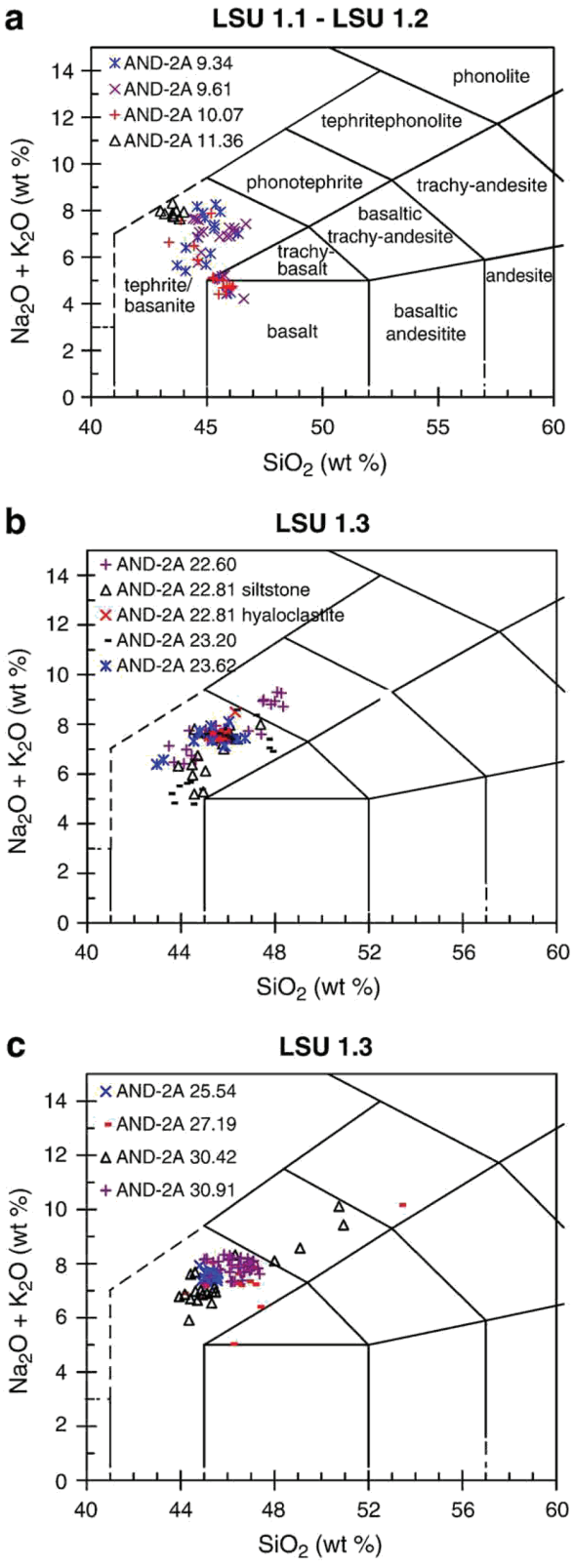


**Figure 13.** Electron microprobe composition of glasses found as LSU 1 clasts plotted on the Total Alkali versus Silica diagram (Le Bas et al., 1986). a) LSU 1.1 and LSU 1.2 samples; b and c) LSU 1.3 samples.

therein). Most of these deposits are more than 50 km from the drill-site and some are significantly above sea-level. Weathering and erosion of this material into the basin by mass flow mechanisms, ice transport or ocean currents would significantly modify volcanic fragments and the deposits should contain a greater diversity of compositions as well as a higher proportion of non-volcanic products. Therefore, they do not represent suitable sources for LSU 1 deposits.

Alternatively, the similarity in composition between the lava clasts recovered from LSU 1 and the lava sampled on Juergens Island lends support to the idea that the Dailey Islands, which are located approximately 13 km to the south–southwest of the SMS drill-site (Figure 1a), could have been the main source of volcanic material in LSU 1. One possibility is that the volcanic material was transported from the Dailey Islands on top of sea-ice and then released into the water column to sink to the seafloor at the drill-site during sea-ice melting. However, this is unlikely given that there are no large dropstones and that delicate bedding structures in poorly indurated sediments are preserved in top-up stratigraphic position, which surely would have been destroyed during ice transport and settling to the seafloor. It is also likely that the components of ice-rafted sediments would show greater heterogeneity in rock types, including a greater range in the composition of volcanic material.

Morphoscopic analysis of clasts in volcanic sands reveal shapes ranging from angular to rounded, indicating different degrees of reworking. Not surprisingly, the sand units that show the greatest effects of reworking have a more heterogeneous composition and higher amounts of terrigenous material (e.g. sample AND-2A 23.62). Only a single layer (AND-2A 30.91) shows features of a near primary pyroclastic deposit. The tephra is mainly composed of highly vesicular sideromelane clasts with irregular and delicate shapes (e.g., Pele's hair), indicating minimal reworking of a primary fall deposit. Furthermore, the homogeneous tephrite composition of the glass (Figure 13c) lends support to an origin from a single eruption. This differs from most of the sand layers which show heterogeneous glass compositions (Figure 13a, b, and c), indicating a mixture of magma sources following similar evolutionary lineages, possible from several eruptions from the same vent or several vents within a single volcanic field.

As a conclusion, we infer that the volcanoclastic sediments in LSU 1 were deposited from volcanic activity near the AND-2A drill-site. A bathymetric study of McMurdo Sound by Barrett et al. (1983) revealed five submarine peaks that rise to depths between 100 and 200 mbsl along the edge of the McMurdo Ice Shelf (locations shown in Figure 1b) that are interpreted to be volcanic cones. Three of the submarine peaks are within about 8 km of the SMS drill-site. Moreover, aeromagnetic surveys indicate that the magnetic high that corresponds to the Cenozoic volcanic deposits of the Dailey Island group also encompass the area around the drill-site (Chiappini et al., 2002). We propose that the Dailey Island volcanic field is much larger than the area encompassed by the islands and extends to the north to include unmapped volcanic vents within the immediate vicinity of the drill-site.

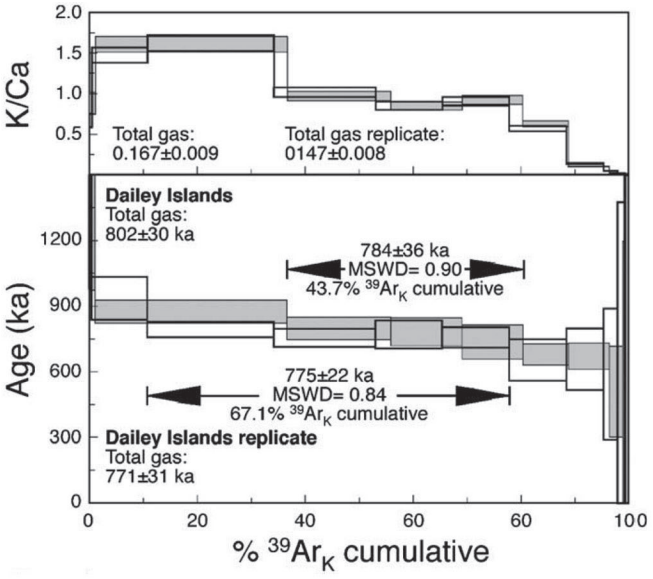


**Figure 14.** Age release and K/Ca spectra of groundmass from the Dailey Islands sample.

### *5.2. Evidence for eruptive style*

Volcanic material of LSU 1 occurs mainly as dense or vesicular glass fragments and lava clasts. Glass fragments range from blocky and cuspate shards to vesicular sideromelane clasts. The glass occurs in a variety of types of sideromelane or tachylite with a wide range in vesicularity, from dense shards to frothy fragments. Highly vesicular glass indicates fragmentation dominated by exsolution and expansion of magmatic gas, whereas blocky and less vesicular glass is indicative of fragmentation dominated by quench processes (Fisher and Schmincke, 1984; Heiken and Wohletz, 1985; Morrissey et al., 2000). Clast morphology and vesicularity support an interpretation for their formation under a diverse range of fragmentation processes consistent with a transitional environment including subaerial and shallow water conditions.

Typical subaerial eruptions that produce pyroclasts similar to those found in LSU 1 are Strombolian and Hawaiian type, which are characterized by mildly basaltic explosive activity. Strombolian eruptions produce discharge of discrete magma bursts releasing magmatic volatiles and produce significant amounts of pyroclasts. Hawaiian eruptions are similar to Strombolian but the bursts of released magmatic volatiles sustain continuous lava fountains (Vergniolle and Mangan, 2000). Pyroclasts produced during Strombolian activity range from variably vesicular scoria fragments to very fluidal (tachylite and sideromelane) fragments. The ash formed during fire-fountaining is carried downwind from the top of the eruptive jet. These particles chill quickly into small glassy black spheres or teardrop shapes called Pele's tears. The teardrop shapes are sometimes drawn out as long filaments by gas, the tails of which can break off to produce Pele's hair (Figure 7h, AND-2A 30.91). The ejecta have a limited dispersal, usually within a few kilometers from the vent. Lava effusion and rootless lava flows accompany these activities.

The presence of some hyaloclastite deposits at different levels in LSU 1 (Table 1) formed of angular, vesicle-free glass shards is typical of magma–water interaction in subaqueous eruptions (Morrissey et al., 2000). The presence of both vesicular and dense fragments in some layers may indicate emergent eruptions from a vent or fissure very close to sea level. In such an environment, magma fragmentation occurs by interaction with seawater and/or by exsolution of volatiles (i.e. Surtseyan type eruptions; White and Houghton, 2000 and references therein).

### *5.3. Evidence for shallow water depths from sedimentary features*

A striking feature of the LSU 1 clastic record is the occurrence of ooliths that, although minor in terms of abundance with respect to other components, are found within the whole LSU 1 deposits (Figure 8a–h). They are characterized by an internally layered coating (for which a silicate composition is inferred on the basis of optical properties and shape) around a core of quartz, as well as around angular fragments of lava, tachylite, colorless glass or sideromelane. It is noteworthy that these core fragment types are the same as those of the sand in which the ooliths are found, indicating an intrabasinal origin for the ooliths. Additionally, some of the glass-cored fragments have highly irregular shapes and preserve primary features such as fragile vesicle walls, ruling out a prolonged period of transport and reworking. The concentric pattern within the coating material and the subspherical shape of the ooliths (irrespective of the original, often irregular morphology of the core fragment) point to a genesis in a shallow marine environment, in analogy with the modern carbonate ooliths, for which a formation in a shallow-water environ-

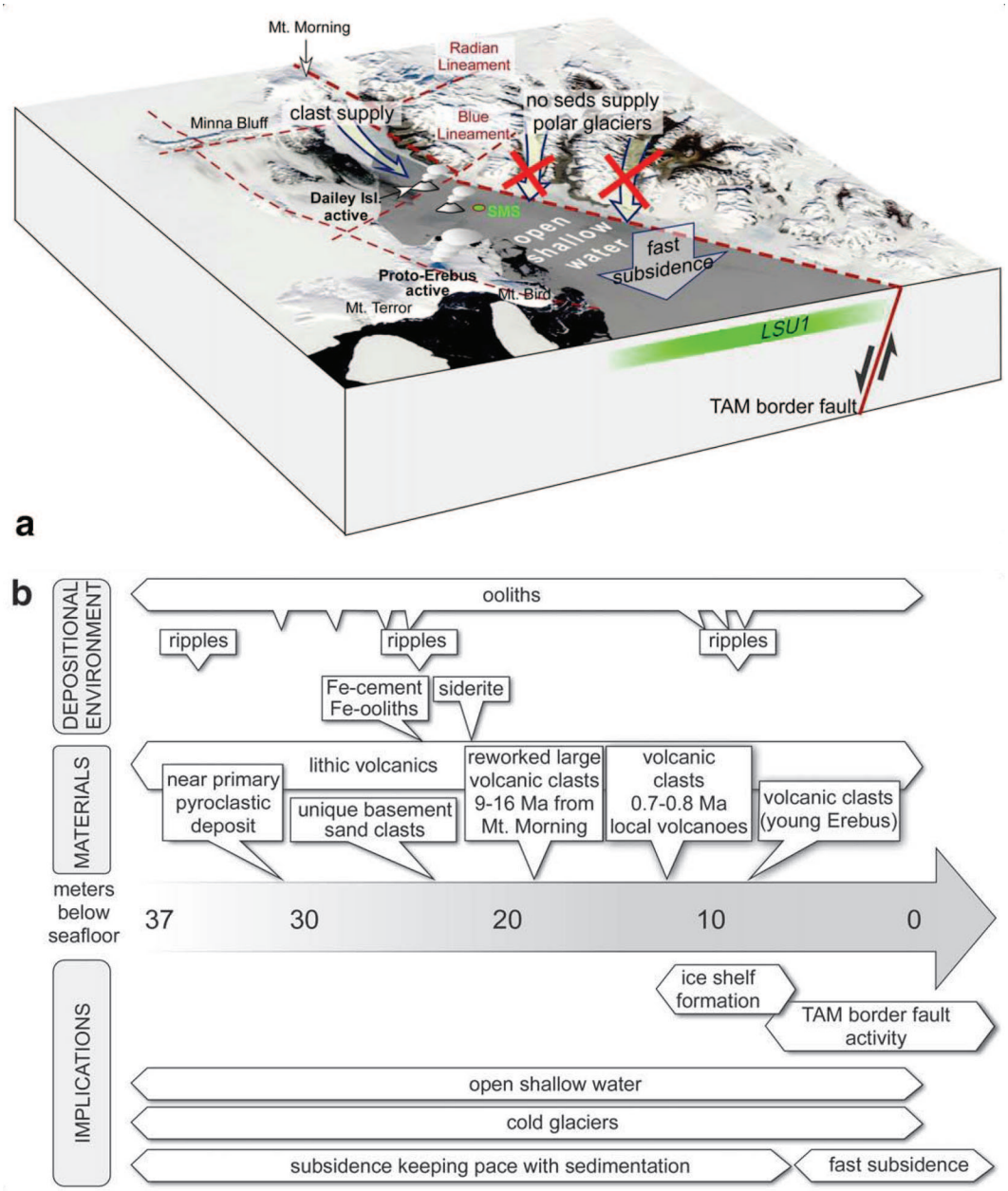


**Figure 15.** Sketch block diagram (a) and a composite cartoon (b) illustrating the overall paleoenvironmental and tectonic setting for the McMurdo Sound area during the Pleistocene time as inferred on the basis of LSU 1 data. Faults redrawn after Paulsen and Wilson (2009).

ment is generally accepted in the literature (Flügel, 2004 and references therein). Most modern ooliths form in shallow waters which are regularly agitated over a long period of time by waves and/or currents (high-energy ooliths, typically characterized by concentric laminae of tangentially arranged crystals). Ooliths may also form in marginal-marine or non-marine shallow water low energy settings (quiet-water ooliths, for which radial or radial-fibrous patterns are common).

Alternatively, these unusual grains might be interpreted as accretionary/armored lapilli formed during hydrovolcanic eruptions. However, this hypothesis is not likely due to the following observations: i) quartz grains, for which an extrabasinal origin is likely, constitute the core of a relevant percentage of the LSU 1 ooliths; ii) the ash plastering around a crystal, pumice or lithic fragment during eruptions usually forms an isopachous rind that mimics the shape of the core (Fisher and Schmincke, 1984, Figure 5.5; Schmincke, 2004, Figure 10.12), which is inconsistent with the irregular thickness of the oolith coatings in LSU 1; iii) if they were armored lapilli, the fine crystalline coating would represent devitrified (recrystallized) ash, however many of the core fragments are composed of fresh glass (in sharp contact with the coating) and it is likely that they would also be partially if not wholly devitrified; iv) the largest crystals within the coating commonly exhibit unbroken elongate shapes whereas irregular shard-like shapes typical of ash coating in armored lapilli were not observed; v) armored lapilli often occur as layers in hydroclastic deposits (Fisher and Schmincke, 1984) and their preservation as isolated grains would be unusual.

Another significant feature, although of limited occurrence in LSU 1, is a siderite layer identified at the transition between a vitroclastic deposit and a volcanic sandstone (LSU 1.3 at 22.81 mbsf). Siderite is most commonly found in non-marine sediments due to the high-carbonate and low-sulfide activity necessary for its precipitation. It may also originate in marine ironstones mostly as a later diagenetic cement (Tucker, 2001), but this was not seen elsewhere in the core and is considered less likely.

Some reddish, oxidized layers are found in the lower part of LSU 1, such as the volcanic sandstone bed at 23.04–23.70 mbsf, which is characterized by a reddish upper portion. Here, the red color is due to a lobate pore-lining cement, iron-rich and variably enriched in other elements (Si, Al, Ti and minor P, Ca and K; Figure 10a) and amorphous

according to XRD analysis. Given the occurrence of Fe-dominated isopachous rims (FeO% ≈ 90 wt.%) growing on the Fe-rich pore-lining lobes (Figure 10b), and of Fe-ooliths with an outer shell of the same composition as the cement (Figure 10c), a multi-stage process of precipitation from a Fe-rich fluid in a shallow water environment can be inferred. Ooliths made of iron minerals (e.g. alternating hematite and chamosite) are a common feature of Phanerozoic ironstones and indicate shallow agitated waters, such as those of Ordovician western Europe developed on marine shelves during phases of sediment starvation at times of relative sea-level rise (Tucker, 2001). Ooliths composed of amorphous iron oxides and/or hydroxides with admixed silica are reported from a modern shallow-marine volcanic setting, and they are interpreted as accretionary bodies formed after direct precipitation (rather than mechanical accretion) from iron- and silica-rich exhalative fluids rising up through the substrate (Heikoop et al., 1996). Sturesson et al. (2000) also suggest a genetic process in close association with active volcanism for the Ordovician iron ooids in northern Europe. We propose that the alteration of volcanic ash and lavas, which is capable of supplying considerable amounts of iron, was the major source of iron for the pore-lining cement and Fe-ooliths in LSU 1 sediments, and that the latter formed in a shallow water environment.

In summary, the occurrence of ooliths throughout the whole LSU 1, including layers containing siderite, Fe-rich cement and Fe-ooliths, along with the occurrence of shallow water diatoms (*Paralia sulcata* and a single fragment of *Cocconeis fasciolata* found in the interval 0–44.06 mbsf, Taviani et al., 2008) indicate that sediments for the whole of LSU 1 were deposited in shallow waters agitated by waves. One important implication for this conclusion is that sea-ice cover in this area could not have been present year-round, as to allow (almost) primary deposition of volcanogenic materials and significant wave motion.

### *5.4. Evidence for shallow water depths from other sedimentary structures*

As for the LSU 1 sedimentary facies, the successions are characterized by intervals of asymmetrically rippled glass-rich moderately- to well-sorted volcanic sands and sandstones (e.g. 9.02–9.86, 24.90–25.27 and 36.65–36.85 mbsf) and poorly-sorted sandy breccias to pebbly sandstones and mudstones, ranging from massive to coarsening-up or fining-up. These structures indicate different depositional processes, some of which are diagnostic of a shallow shelf environment.

The more poorly-sorted, massive to coarsening or fining up deposits were laid down by mass flows ranging from more viscous sub-marine debris flows to less viscous turbidity currents (e.g. Sohn, 1997; Mutti et al., 1999; Shanmugam, 2000, 2002; Mutti et al., 2003; Mohrig and Marr, 2003). It is common for these currents, in submarine settings, to be thin but widespread. They are also extremely common in volcanic settings given the episodic but abundant supply of sediment (Schneider et al., 2001). Compositionally, these beds show the widest range in clast types and are more likely to contain basement materials. These were very likely brought in by aeolian processes to the sea ice surface (Atkins and Dunbar, 2009), deposited when melted and then mixed by the sediment gravity flows with the more proximal volcanic sediment.

The rippled sands and hummocky cross-stratification are more diagnostic of water depth and, in this case, have been interpreted to have formed at shallow to mid-shelf depths. The ripple cross-laminations are asymmetrical indicating deposition by current, but are not part of fining upward Bouma sequences typical of turbidites (Figure 12). Therefore, we interpret deposition by a current, rather than by wave oscillations, probably in currents generated by storm set up conditions. The hummocky cross-stratification is comprised of cross-cutting hummocks and swales with clear erosive contacts (Figure 11). These are more similar to true oscillatory wave-generated bedforms from shallow marine shelf depths, possibly combined with unidirectional flow of turbidite currents (e.g. Myrow et al., 2002, 2008; Lamb et al., 2008) than the antidune forms that can occur in deeper water turbidites (e.g. Mulder et al., 2009). The ripple cross-lamination and hummocky cross-stratification structures occur intermittently within the deposit indicating that water depths were not shallow enough to be affected by daily wave activity but are in water depths above storm wave base in the basin, possibly the deeper side of storm wave base.

Their composition generally tends to be more glass-rich, possibly reflecting either a lighter, more easily stirred size fraction, or else sediment influxes from local eruptions leaving little else to be reworked by the waves. Waves are effective at stirring up sediment from the sea floor, but are ineffective at lateral transport unless combined with currents from tides or storm set up (Allen, 1997). The availability of lighter, abundant grains to be transported would affect the distribution of the sedimentary structures.

Calculating the depth of the storm wave base depends on the scale of the storms, the latitude of the deposits, local bathymetry, and local currents. The transition from wave transport to deeper water geostrophic currents should be expected in < 100 m water depth (Allen, 1997). However, sea-ice has a damping effect on wave generation (Butler, 1999) limiting wave generation to open water conditions. Multiple reflection from changes in sea-ice thickness attenuates the transmission of waves generated in open water waves into an area covered by sea-ice except for very long period waves (Squire, 2007; Squire and Williams, 2008). Modern currents in McMurdo Sound near the drill-site were not measured, but were modeled based on nearby data (Jacobs, 1989; Limeburner et al., in press). They were of limited velocity, and no effects from currents were observed during the drilling process (Falconer et al., 2008). Thus, the infrequency of rippled and hummocky cross-stratified sandstones may be due to limited open water conditions, or else significantly shallower depths with storm waves generated in nearby open water propagated through the sea-ice stirring up the sea floor sediments. Another possibility is that a local eruption caused blanketing of the sea-ice with volcanic material, which accelerated melting to form small ephemeral areas of open water. This may explain why the rippled sands tend to be more glass-rich. The overall conclusion here is that LSU 1 was deposited in water that was probably significantly shallower than 100 m, and not too far from several volcanic vents.

## 6. Implications for subsidence history of the southern Victoria Land Basin

The AND-2A site is located at the southernmost end of the Victoria Land Basin. Evidence for shallow water sedimentation is presented in this paper for the entire thickness of LSU 1. Furthermore, the lithostratigraphic units lying beneath LSU 1 were also deposited in shallow water conditions (Fielding et al., 2008b). These results contrast strikingly with the present water depth at the drill-site (close to 400 m), which lead us to infer a rapid recent basin subsidence of almost 300 m, after deposition of LSU 1.

To reconcile these contrasting pieces of evidence, deep incision by the Koettlitz Glacier during the last glacial maximum could be invoked. However, this explanation is unlikely given that large parts of the Dailey Islands are still uneroded and the subaerial and nearshore marine sediments from LSU 1 would have been removed rather than preserved. Another alternative possibility is represented by the volcanic loading either by the local Dailey Islands or by Mt. Erebus, yet the Dailey Islands are too small and too far from the drill-site to cause significant subsidence. Mt. Erebus seems more likely, but seismic reflection profiles show that the SMS drill-site lies several kilometers beyond the Erebus moat (Fielding et al., 2008a). A third possibility is to invoke large scale transport of LSU 1 as a single block by glacial ice or atop sea-ice. This process is also unlikely, given the good preservation of fragile sedimentary structures in top-up stratigraphic position. Furthermore, other shallow water deposits are found immediately underlying LSU 1 (Fielding et al., 2008b).

The deepening of the basin linked to very recent tectonic subsidence appears to be the most likely explanation. As a speculation, subsidence could be controlled by faults in the Discovery Accommodation

Zone (Wilson, 1995, 1999), a Late Cenozoic transverse zone that coincides with a prominent offset of the Transantarctic Mountains rift flank and the voluminous volcanism of the Erebus Volcanic Province (Figure 15). In this overall framework, Pleistocene activity of the faults intersecting the Mt. Morning area might have been responsible for supplying the large lava clasts found between 18 and 19 mbsf and dated at 16.1 and 9.5 Ma. Therefore, the Ross Ice Shelf could not have been stable until recently, to allow clast discharge in the uppermost sedimentary unit (LSU 1) in the southernmost part of the basin.

Although seismic studies do not show unequivocal evidence for large-scale faulting in the immediate vicinity of the SMS drill-site (Stern, 1984; Fielding et al., 2008a), Pliocene–Pleistocene age faulting has been recently documented in the Terror Rift (Hall et al., 2007; Henrys et al., 2007), including normal faults that cut Pleistocene strata in the AND-2A (Paulsen et al., 2008) and AND-1B cores (Wilson et al., 2007). Paulsen and Wilson (2009) combine this information with their study of the structure and age of volcanic fissures on Mount Morning to suggest that a normal-fault to strike-slip fault regime could be active today. While further speculation on the specific mechanism for subsidence is beyond the scope of this paper, it is evident from our findings that an active field of shallow volcanic seamounts and islands must have been present in close proximity to the drill-site. Furthermore, based on the similarity in compositions and age, as well as findings from bathymetric (Barrett et al., 1983) and aeromagnetic (Chiappini et al., 2002) surveys, this field most likely represents a northern extension of the same activity that formed the Dailey Islands. In this scenario, the stabilization of the ice shelf could then be related to the build-up of the Dailey Islands, which were acting as pinning points for continental ice flowing into the Ross Sea. The shelf in turn is shielding Dailey Islands from wave erosion, helping these small volcanic islands to survive to the present.

**Acknowledgments — The a**uthors are grateful to Co-Chiefs F. Florindo and D. Harwood and the Science Team (http://www.andrill.org) of the SMS ANDRILL Project. A. Cavallo is kindly acknowledged for the assistance during microprobe analyses. KP thanks the Department of Geological Sciences at the University of Canterbury (NZ) for the support on this project. PDC thanks A. Di Roberto and M. Pompilio for their helpful discussions. LB kindly acknowledges the helpful comments on siliciclastic sediments by L. Pandolfi. We also thank two anonymous reviewers for their helpful critiques that improved the manuscript.

The ANDRILL project is a multinational collaboration between the Antarctic Programs of Germany, Italy, New Zealand, and the United States. Antarctica New Zealand is the project operator, and it has developed the drilling system in collaboration with Alex Pyne at Victoria University of Wellington and Webster Drilling and Exploration Ltd. Antarctica New Zealand supported the drilling team at Scott Base, and Raytheon Polar Services supported the Science team at McMurdo Station and the Crary Science and Engineering Center. Scientific support was provided by the ANDRILL Science Management Office, University of Nebraska–Lincoln. Scientific studies are jointly supported by the U.S. National Science Foundation, NZ Foundation for Research, the Italian Antarctic Research Program (PNRA), the German Science Foundation, and the Alfred Wegener Institute. LB benefited of a postdoc grant from PNRA.

## References

**Acton et al., 2008** • G. Acton, J. Crampton, G. Di Vincenzo, C.R. Fielding, F. Florindo, M. Hannah, D. Harwood, S. Ishman, K. Johnson, L. Covane, R. Levy, B. Lum, M.C. Marcano, S. Mukasa, C. Ohneiser, M. Olney, C. Riesselman, L. Sagnotti, C. Stefano, E. Strada, M. Taviani, E. Tuzzi, K.L. Verosub, G.S. Wilson, and M. Zattin, Preliminary integrated chronostratigraphy of the AND-2A core, ANDRILL Southern McMurdo Sound Project. In: D.M. Harwood, F. Florindo, F. Talarico, and R.H. Levy, editors, *Studies from the ANDRILL, Southern McMurdo Sound Project, Antarctica*, *Terra Antartica,* vol. 15 (1/2) (2008).

**Allen, 1997** • P.A. Allen, *Earth Surface Processes,* Blackwell Science, Oxford (1997).

**Anderson et al., 1984** • J.B. Anderson, C.F. Brake, and N.C. Myers, Sedimentation on the Ross Sea continental shelf, *Marine Geology* **57** (1984), pp. 295–333.

**Atkins and Dunbar, 2009** • C.B. Atkins and G.B. Dunbar, Aeolian sediment flux from sea ice into Southern McMurdo Sound (SMS), Antarctica, *Global and Planetary Change* **69** (2009), pp. 133–141.

**Barrett, 1987** • P.J. Barrett, Oligocene sequence cored at CIROS-1, western McMurdo Sound, *New Zealand Antarctic Record* **7** (1987), pp. 1–17.

**Barrett et al., 1983** • P.J. Barrett, A.R. Pyne, and A.J. Macpherson, Observations of the sea floor of McMurdo Sound and Granite Harbour, *New Zealand Antarctic Record* **5** (2) (1983), pp. 16–22.

**Behrendt et al., 1991** • J.C. Behrendt, W.E. LeMasurier, A.K. Cooper, F. Tessensohn, A. Trehu, and D. Damaske, Geophysical studies of the West Antarctic Rift System, *Tectonics* **10** (6) (1991), pp. 1257–1273.

**Butler, 1999** • E.R.T. Butler, Process environments on modern and raised beaches in McMurdo Sound, Antarctica, *Marine Geology* **162** (1999), pp. 105–120.

**Chiappini et al., 2002** • M. Chiappini, F. Ferraccioli, E. Bozzo, and D. Damaske, Regional compilation and analysis of aeromagnetic anomalies for the Transantarctic Mountains–Ross Sea sector of the Antarctic, *Tectonophysics* **347** (2002), pp. 121–137.

**Cooper et al., 2007** • A.F. Cooper, L.J. Adam, R.F. Coulter, G.N. Eby, and W.C. McIntosh, Geology, geochronology and geochemistry of a basanitic volcano, White Island, Ross Sea, Antarctica, *Journal of Volcanology and Geothermal Research* **165** (2007), pp. 189–216.

**Denton and Marchant, 2000** • G.H. Denton and D.R. Marchant, The Geologic basis for a reconstruction of a grounded ice sheet in McMurdo Sound, Antarctica, at the Last Glacial Maximum, *Geografiska Annalar* **82** (A(2–3)) (2000), pp. 167–211.

**Dickinson, 1970** • W.R. Dickinson, Interpreting detrital modes of greywacke and arkose, *Journal of Sedimentary Petrology* **40** (1970), pp. 695–707.

**Dickinson, 1985** • W.R. Dickinson, Interpreting provenance relations from detrital modes of sandstones. In: G.G. Zuffa, editor, *Provenance of arenites:* NATO Advanced Study Institutes series, D. Reidel Publishing Company, Dordrecht (1985), pp. 333–362.

**Di Vincenzo and Skála, 2009** • G. Di Vincenzo and R. Skála, $^{40}Ar$–$^{39}Ar$ laser dating of tektites from the Cheb Basin (Czech republic): Evidence for coevality with moldavites and influence of the dating standard on the age of the Ries impact, *Geochimica et Cosmochimica Acta* **73** (2) (2009), pp. 493–513; doi: 10.1016/j.gca.2008.10.002.

**Di Vincenzo et al., 2009** • G. Di Vincenzo, L. Bracciali, P. Del Carlo, K. Panter, and S. Rocchi, $^{40}Ar$–$^{39}Ar$ laser dating of volcanogenic products from the AND-2A core (ANDRILL Southern McMurdo Sound Project, Antarctica), *Bulletin of Volcanology* (2009) sub judice.

**Elliot et al., 1999** • D.H. Elliot, T.H. Fleming, P.R. Kyle, and K.A. Foland, Long-distance transport of magmas in the Jurassic Ferrar Large Igneous Province, Antarctica, *Earth and Planetary Science Letters* **167** (1999), pp. 89–104.

**Esser et al., 2004** • R.P. Esser, P.R. Kyle, and W.C. McIntosh, $^{40}Ar$–$^{39}Ar$ dating of the eruptive history of Mount Erebus, Antarctica: Volcano evolution, *Bulletin of Volcanology* **66** (2004), pp. 671–686; doi: 10.1007/s00445-00004-00354-x

**Falconer et al., 2008** • T.A. Falconer, A. Pyne, D. Wilson, R. Levy, S. Nielsen, S. Petrushak, and the ANDRILL-SMS Science Team, Operations overview for the ANDRILL Southern McMurdo Sound Project, Antarctica, *Terra Antartica* **15** (1/2) (2008).

**Fargo et al., 2008** • A.J. Fargo, W.C. McIntosh, N.W. Dunbar, and T.I. Wilch, $^{40}Ar$–$^{39}Ar$ geochronology of Minna Bluff, Antarctica: Timing of Mid-Miocene glacial erosional events within the Ross Embayment, *EOS, Transactions of the American Geophysical Union* **89**(53) (2008) Fall Meet. Suppl., Abstract V13C-2127.

**Fielding et al., 2008a** • C.R. Fielding, J. Whittaker, S.A. Henrys, T.J. Wilson, and T.R. Naish, Seismic facies and stratigraphy of the Cenozoic succession in McMurdo Sound, Antarctica: Implications for tectonic, climatic and gla-

cial history, *Paleogeography, Paleoclimatology, Palaeoecology* **260** (2008), pp. 8–29.

**Fielding et al., 2008b** • C.R. Fielding, C.B. Atkins, K.N. Bassett, G.H. Browne, G.B. Dunbar, B.D. Field, T.D. Frank, K.S. Panter, S.F. Pekar, L.A. Krissek, and S. Passchier, Sedimentology and stratigraphy of the AND-2A core, ANDRILL Southern McMurdo Sound, Project, Antarctica. In: D.M. Harwood, F. Florindo, F. Talarico, and R.H. Levy, editors, *Studies from the ANDRILL, Southern McMurdo Sound Project, Antarctica*, *Terra Antartica,* vol. 15 (1/2) (2008).

**Finn et al., 2005** • C.A. Finn, R.D. Müller, and K.S. Panter, A Cenozoic diffuse alkaline magmatic province (DAMP) in the SW Pacific without rift or plume origin, *Geochemistry, Geophysics, Geosystems ($G^3$)* **6** (1) (2005), p. Q02005; doi: 10.1029/2004GC000723

**Fisher and Schmincke, 1984** • R.V. Fisher and H.-U. Schmincke, *Pyroclastic Rocks,* Springer, Berlin (1984) 472 pp.

**Florindo et al., 2008** • F. Florindo, D. Harwood, R. Levy, and SMS Project Science Team, ANDRILL's Success during the 4th International Polar Year, *Scientific Drilling* **6** (2008), pp. 29–31.

**Flügel, 2004** • E. Flügel, *Microfacies of carbonate rocks—Analysis, interpretation and application,* Springer (2004) 976 pp.

**Gamble et al., 1986** • J.A. Gamble, P.J. Barrett, and C.J. Adams, Basaltic clasts from Unit 8, *Bulletin of New Zealand DSIR* **237** (1986), pp. 145–152.

**Gazzi, 1966** • P. Gazzi, Le Arenarie del Flysch Sopracretaceo dell'Appennino Modenese: Correlazioni con il Flysch di Monghidoro, *Mineralogica e Petrografica Acta* **12** (1966), pp. 69–97.

**Hall et al., 2007** • J.M. Hall, T.J. Wilson, and S.A. Henrys, Structure of central Terror Rift, western Ross Sea, Antarctica. In: A.K. Cooper and C.R. Raymond *et al.*, editors, *Antarctica: A keystone in a changing world—Online proceedings of the 10th ISAES X, USGS Open-File Report 2007-1047, Short Research Paper,* vol. 108 (2007); doi: 10.3133/of2007-1047.srp108.

**Harpel et al., 2004** • C.J. Harpel, P.R. Kyle, R.P. Esser, W.C. McIntosh, and D.A. Caldwell, $^{40}Ar$–$^{39}Ar$ dating of the eruptive history of Mount Erebus, Antarctica: Summit flows, tephra, and caldera collapse, *Bulletin of Volcanology* **66** (2004), pp. 687–702.

**Harwood et al., 2008** • D.M. Harwood, F. Florindo, F. Talarico, R.H. Levy, G. Acton, C. Fielding, K. Panter, T. Paulsen, and M. Taviani, Synthesis of the Initial Scientific Results of the ANDRILL Southern McMurdo Sound Project, Victoria Land Basin, Antarctica. In: D.M. Harwood, F. Florindo, F. Talarico, and R.H. Levy, editors, *Studies from the ANDRILL, Southern McMurdo Sound Project, Antarctica*, *Terra Antartica,* vol. 15 (1/2) (2008).

**Heiken and Wohletz, 1985** • G.H. Heiken and K.H. Wohletz, *Volcanic ash,* University of California Press, Berkeley, CA (1985).

**Heikoop et al., 1996** • J.M. Heikoop, C.J. Tsujita, M.J. Risk, T. Tomascik, and A.J. Mah, Modern iron ooids from a shallow-marine volcanic setting: Mahengetang, Indonesia, *Geology* **24** (8) (1996), pp. 759–762.

**Henrys et al., 2007** • S.A. Henrys, T.J. Wilson, J. Whittaker, C.R. Fielding, J. Hall, and T.R. Naish, Tectonic history of Mid-Miocene to present southern Victoria Land Basin, inferred from seismic stratigraphy, in McMurdo Sound, Antarctica. In: A.K. Cooper and C.R. Raymond *et al.*, editors, *Antarctica: A keystone in a changing world—Online proceedings of the 10th ISAES X, USGS Open-File Report 2007-1047, Short Research Paper,* vol. 049 (2007); doi: 10.3133/of2007-1047.srp049.

**Jacobs, 1989** • S.S. Jacobs, Marine controls on modern sedimentation on the Antarctic continental shelf, *Marine Geology* **85** (1989), pp. 121–153.

**Jourdan and Renne, 2007** • F. Jourdan and P.R. Renne, Age calibration of the Fish Canyon sanidine $^{40}Ar$–$^{39}Ar$ dating standard using primary K–Ar standard, *Geochimica et Cosmochimica Acta* **71** (2007), pp. 387–402.

**Kelly et al., 2008** • P.J. Kelly, P.R. Kyle, N.W. Dunbar, and K.W.W. Sims, Geochemistry and mineralogy of the phonolite lava lake, Erebus volcano, Antarctica: 1972–2004 and comparison with older lavas, *Journal of Volcanology and Geothermal Research* **177** (2008), pp. 589–605; doi: 10.1016/j.jvolgeores.2007.11.025

**Kyle, 1990** • P.R. Kyle, Erebus volcanic province; Summary, *Volcanoes of the Antarctic Plate and Southern Oceans* **48** (1990), pp. 81–88.

**Kyle and Cole, 1974** • P.R. Kyle and J.W. Cole, Structural control of volcanism in the McMurdo Volcanic Group, Antarctica, *Bulletin of Volcanology* **38** (1) (1974), pp. 16–25.

**Kyle et al., 1992** • P.R. Kyle, J.A. Moore, and M.F. Thirlwall, Petrologic evolution of anorthoclase phonolite lavas at Mount Erebus, Ross Island. Antarctica, *Journal of Petrology* **33** (4) (1992), pp. 849–875.

**Lamb et al., 2008** • M.P. Lamb, P.M. Myrow, C. Lukens, and K. Houck, Deposits from wave-influenced turbidity currents: Pennsylvanian Minturn Formation, Colorado, U.S.A., *Journal of Sedimentary Research* **78** (2008), pp. 480–498.

**Lawrence et al., 2009** • K.P. Lawrence, L. Tauxe, H. Staudigel, C.G. Constable, A. Koppers, W. McIntosh, and C.L. Johnson, Paleomagnetic field properties at high southern latitude, *Geochemistry, Geophysics, Geosystems ($G^3$)* **10** (1) (2009); doi: 10.1029/2008GC002072.

**Le Bas et al., 1986** • M.J. Le Bas, R.W. Le Maitre, A. Streckeisen, and B.A. Zanettin, Chemical classification of volcanic rocks based on the total alkali-silica diagram, *Journal of Petrology* **27** (1986), pp. 745–750.

**LeMasurier and Thomson, 1990** • W.E. LeMasurier and J.W. Thomson, editors, *Volcanoes of the Antarctic Plate and Southern Ocean*, *Antarctic Research Series*, American Geophysical Union, Washington D.C. (1990) , 487 pp.

**Limeburner et al., in press** • R. Limeburner, R. Beardsley, and S. Whelan, *ANDRILL moored data 2006 Report.* Woods Hole Oceanographic Institute, in press.

**Mankinen and Cox, 1988** • E.A. Mankinen and A. Cox, Paleomagnetic investigation of some volcanic rocks from the McMurdo Volcanic Province, Antarctica, *Journal of Geophysical Research* **93** (11) (1988), pp. 599–612.

**McIntosh, 1998** • W.C. McIntosh, $^{40}Ar/^{39}Ar$ geochronology of volcanic clasts and pumice in CRP-1 core, Cape Roberts, Antarctica, *Terra Antartica* **5** (1998), pp. 683–690.

**McIntosh, 2000** • W.C. McIntosh, $^{40}Ar$–$^{39}Ar$ geochronology of tephra and volcanic clasts in CRP-2A, Victoria Land Basin, Antarctica, *Terra Antartica* **7** (4) (2000), pp. 621–630.

**McPhie et al., 1993** • J. McPhie, M. Doyle, and R. Allen, *Volcanic textures*, Centre for ore deposit and exploration studies, University of Tasmania (1993) 198 pp.

**Mohrig and Marr, 2003** • D. Mohrig and J.G. Marr, Constraining the efficiency of turbidity current generation from submarine slides, slumps and debris flows using laboratory experiments, *Journal of Marine and Petroleum Geology* **20** (2003), pp. 883–899.

**Morrissey et al., 2000** • M. Morrissey, B. Zimanowski, K. Wohletz, and R. Buettner, Phreatomagmatic fragmentation. In: H. Sigurdsson, B. Houghton, S. McNutt, H. Rymer, and J. Stix, editors, *Encyclopedia of Volcanoes*, Academic Press, San Diego, CA (2000), pp. 431–445.

**Mulder et al., 2009** • T. Mulder, P. Razin, and J.C. Faugeres, Hummocky cross-stratification-like structures in deep-sea turbidites: Upper Cretaceous Basque basins (Western Pyrenees, France), *Sedimentology* **56** (2009), pp. 997–1015.

**Mutti et al., 1999** • E. Mutti, R. Tinterri, E. Remacha, N. Mavilla, S. Angella, and L. Fava, An introduction to the analysis of ancient turbidite basins from an outcrop perspective, *AAPG Course Note* **39** (1999), p. 93.

**Mutti et al., 2003** • E. Mutti, R. Tinterri, G. Benevelli, D. di Biase, and G. Cavanna, Deltaic, mixed and turbidite sedimentation of ancient foreland basins, *Marine and Petroloeum Geology* **20** (2003), pp. 733–755.

**Myrow et al., 2002** • P.M. Myrow, W. Fischer, and J.W. Goodge, Wave-modified turbidites: combined-flow shoreline and shelf deposits, Cambrian, Antarctica, *Journal of Sedimentary Reasearch* **72** (5) (2002), pp. 641–656.

**Myrow et al., 2008** • P.M. Myrow, C. Lukens, M.P. Lamb, and K. Houck, Dynamics of a transgressive prodeltaic system: implications for geography and climate within a Pennsylvanian intracratonic basin, Colorado, U.S.A., *Journal of Sedimentary Research* **78** (2008), pp. 512–528.

**Neuendorf et al., 2005** • K.K.E. Neuendorf, J.P.J. Mehl, and J.A. Jackson, editors, *Glossary of Geology* (5th edition), American Geological Institute, Alexandria (VA) (2005) 779 pp.

**Oppenheimer and Kyle, 2008** • C. Oppenheimer and P. Kyle, Volcanology of Erebus volcano, Antarctica, *Journal of Volcanolology and Geothermal Research* **177** (3) (2008), pp. v–vii; doi: 10.1016/j.jvolgeores.2008.10.006

**Panter et al., 2008** • K.S. Panter, F. Talarico, K. Bassett, P. Del Carlo, B. Field, T. Frank, S. Hoffman, G. Kuhn, L. Reichelt, S. Sandroni, M. Taviani, L. Bracciali, G. Cornamusini, H. von Eynatten, and R. Rocchi, Petrologic and Geochemical Composition of the AND-2A Core, ANDRILL Southern McMurdo Sound Project, Antarctica. In: D.M. Harwood, F. Florindo, F. Talarico, and R.H. Levy, editors, *Studies from the ANDRILL, Southern McMurdo Sound Project, Antarctica*, *Terra Antartica,* vol. 15 (1/2) (2008).

**Paulsen and Wilson, 2009** • T.S. Paulsen and T.J. Wilson, Structure and age of volcanic fissures on Mount Morning: a new constraint on Neogene to con-

temporary stress in the West Antarctic Rift, southern Victoria Land, Antarctica, *Geological Society of America Bulletin* **121** (7/8) (2009), pp. 1071–1088.

**Paulsen et al., 2008** • T. Paulsen, C. Millan, S. Pierdominici, T. Wilson, Scott Drew, and the ANDRILL-SMS Science Team, Fracture logging of the AND-2A core, ANDRILL Southern McMurdo Sound Project, Antarctica. In: D.M. Harwood, F. Florindo, F. Talarico, and R.H. Levy, editors, *Studies from the ANDRILL, Southern McMurdo Sound Project, Antarctica*, *Terra Antartica,* vol. 15 (1/2) (2008).

**Pettijohn et al., 1987** • F. Pettijohn, P. Potter, and R. Siever, *Sand and Sandstone,* Springer-Verlag, New York (1987).

**Renne et al., 1998** • P.R. Renne, C.C. Swisher, A.L. Deino, D.B. Karner, T.L. Owens, and D.J. DePaolo, Intercalibrations of standards, absolute ages and uncertainties in $^{40}Ar$–$^{39}Ar$ dating, *Chemical Geology* **145** (1998), pp. 117–152.

**Rocchi et al., 2002** • S. Rocchi, P. Armienti, M. D'Orazio, S. Tonarini, J. Wijbrans, and G. Di Vincenzo, Cenozoic magmatism in the western Ross Embayment: Role of mantle plume vs. plate dynamics in the development of the West Antarctic Rift System, *Journal of Geophysical Research* **107** (B9) (2002), p. 2195.

**Rocchi et al., 2003** • S. Rocchi, F. Storti, G. Di Vincenzo, and F. Rossetti, Intraplate strike-slip tectonics as alternative to mantle plume activity for the Cenozoic rift magmatism in the Ross Sea region, Antarctica. In: F. Storti, R.E. Holdsworth, and F. Salvini, editors, *Intraplate strike-slip deformation belts*, Geological Society of London Special Publication, vol. 210 (2003), pp. 158–171.

**Rocchi et al., 2005** • S. Rocchi, G. Di Vincenzo, and P. Armienti, No plume, no rift magmatism in the West Antarctic rift. In: G.R. Foulger, D.L. Anderson, J.H. Natland, and D.C. Presnall, editors, *Plates, Plumes & Paradigms*, SGA Special Paper, vol. 388 (2005), pp. 435–447.

**Schmincke, 2004** • H.U. Schmincke, *Volcanism*, Springer (2004) 324 pp.

**Schneider et al., 2001** • J.L. Schneider, A. Le Ruyet, F. Chanier, C. Buret, J. Ferriere, J.N. Proust, and J.B. Rosseel, Primary or secondary distal volcaniclastic turbidites: How to make the distinction? An example from the Miocene of New Zealand (Mahia Peninsula, North Island), *Sedimentary Geology* **145** (2001), pp. 1–22.

**Shanmugam, 2000** • G. Shanmugam, 50 years of the turbidite paradigm (1950s–1990s): Deep-water processes and facies models, *Marine and Petroleum Geology* **17** (2000), pp. 285–342.

**Shanmugam, 2002** • G. Shanmugam, Ten turbidite myths, *Earth-Science Reviews* **58** (2002), pp. 311–341.

**Squire, 2007** • V.A. Squire, Of ocean waves and sea-ice revisited, *Cold Regions Science and Technology* **49** (2007), pp. 110–133.

**Squire and Williams, 2008** • V.A. Squire and T.D. Williams, Wave propagation across sea-ice thickness changes, *Ocean Modelling* **21** (2008), pp. 1–11.

**Sohn, 1997** • Y.K. Sohn, On traction carpet sedimentation, *Journal of Sedimentary Research* **67** (1997), pp. 502–509.

**Steiger and Jäger, 1977** • R.H. Steiger and E. Jäger, Subcommission on geochronology: Convention on the use of decay constants in geo- and cosmochronology, *Earth and Planetary Sciences Letters* **36** (1977), pp. 359–362.

**Stern, 1984** • Stern, T.A., 1984. A seismic refraction survey near the Dailey Islands, southwestern McMurdo Sound, Antarctica. Geophysics Division Report 98, Department of Scientific and Industrial Research, Wellington, New Zealand.

**Sturesson et al., 2000** • U. Sturesson, J.M. Heikoop, and M.J. Risk, Modern and Palaeozoic iron ooids — A similar volcanic origin, *Sedimentary Geology* **136** (1–2) (2000), pp. 137–146.

**Tamponi et al., 2003** • M. Tamponi, F. Bertoli, F. Innocenti, and L. Leoni, X-ray fluorescence analysis of major elements in silicate rocks using fused glass discs, *Atti della Società Toscana di Scienze Naturali, Memorie Serie A* **107** (2003), pp. 73–80.

**Tauxe et al., 2004** • L. Tauxe, P. Gans, and E.A. Mankinen, Paleomagnetism and $^{40}Ar$–$^{39}Ar$ ages from volcanics extruded during the Matuyama and Brunhes Chrons near McMurdo Sound, Antarctica, *Geochemistry, Geophysics, Geosystems ($G^3$)* **5** (6) (2004); doi: 10.1029/2003GC000656.

**Taviani et al., 2008** • M. Taviani, M. Hannah, D.M. Harwood, S.E. Ishman, K. Johnson, M. Olney, C. Riesselman, E. Tuzzi, R. Askin, A.G. Beu, S. Blair, V. Cantarelli, A. Ceregato, S. Corrado, B. Mohr, S.H.H. Nielsen, D. Persico, S. Petrushak, J.I. Raine, and S. Warny, Palaeontologic characterization of the AND-2A Core, ANDRILL Southern McMurdo Sound Project, Antarctica. In: D.M. Harwood, F. Florindo, F. Talarico, and R.H. Levy, editors, *Studies from the ANDRILL, Southern McMurdo Sound Project, Antarctica*, *Terra Antartica,* vol. 15 (1/2) (2008).

**Tucker, 2001** • M.E. Tucker, *Sedimentary petrology: An introduction to the origin of sedimentary rocks,* Blackwell Science Ltd, Oxford (2001).

**Vergniolle and Mangan, 2000** • S. Vergniolle and M. Mangan, Hawaiian and Strombolian eruptions. In: H. Sigurdsson, B. Houghton, S. McNutt, H. Rymer, and J. Stix, editors, *Encyclopedia of Volcanoes*, Academic Press, San Diego, CA (2000), pp. 447–461.

**White and Houghton, 2000** • J.D.L. White and B. Houghton, Surtseyan and related phreatomagmatic eruptions. In: H. Sigurdsson, B. Houghton, S. McNutt, H. Rymer, and J. Stix, editors, *Encyclopedia of Volcanoes*, Academic Press, San Diego, CA (2000), pp. 495–525.

**Wilch et al., 1993** • T.I. Wilch, D.R. Lux, G.H. Denton, and W.C. McIntosh, Minimal Pliocene–Pleistocene uplift of the dry valleys sector of the Transantarctic Mountains: A key parameter in ice-sheet reconstructions, *Geology* **21** (1993), pp. 841–844.

**Wilson, 1995** • T.J. Wilson, Cenozoic transtension along the Transantarctic Mountains–West Antarctic rift boundary, southern Victoria Land, Antarctica, *Tectonics* **14** (1995), pp. 531–545.

**Wilson, 1999** • T.J. Wilson, Cenozoic structural segmentation of the Transantarctic Mountains rift flank in southern Victoria Land, *Global and Planetary Change* **23** (1–4) (1999), pp. 105–127.

**Wilson et al., 2007** • T. Wilson, T. Paulsen, A. Läufer, C. Millan, and the ANDRILL-MIS Science Team, Fracture logging of the AND-1B core, ANDRILL McMurdo Ice Shelf Project, Antarctica, *Terra Antartica* **14** (2007), pp. 109–328.